Short article

Cell Host & Microbe

Human cytomegalovirus degrades DMXL1 to inhibit autophagy, lysosomal acidification, and viral assembly

Graphical abstract

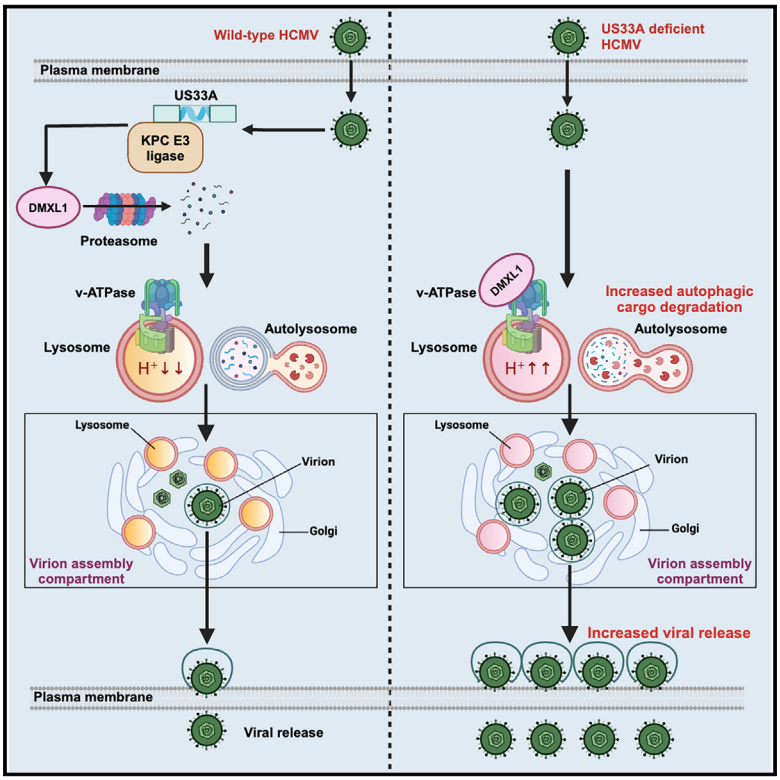

Highlights

- Systematic proteomic definition of the function of seven HCMV proteins
- HCMV US33A hijacks the KPC E3 ligase and is necessary and sufficient to degrade DMXL1
- DMXL1 degradation inhibits lysosomal acidification and autophagic cargo degradation
- DMXL1 degradation inhibits virion assembly compartment formation and viral release

Authors

Hanqi Li, Alice Fletcher-Etherington, Leah M. Hunter, ..., David C. Rubinsztein, Richard J. Stanton, Michael P. Weekes

Correspondence

mpw1001@cam.ac.uk

In brief

Li et al. report that human cytomegalovirus (HCMV) US33A degrades DMXL1, a key regulator of vacuolar acidification, to remodel host lysosomes and autophagy. The US33A protein hijacks the cellular KPC E3 ligase complex, inhibiting HCMV assembly and release, as well as suppressing herpes simplex virus replication.

Li et al., 2024, Cell Host & Microbe *32*, 466–478
April 10, 2024
https://doi.org/10.1016/j.chom.2024.02.013

CellPress

CellPress
OPEN ACCESS

Cell Host & Microbe

Short article

Human cytomegalovirus degrades DMXL1 to inhibit autophagy, lysosomal acidification, and viral assembly

Hanqi Li,[1,2,6] Alice Fletcher-Etherington,[1,2,6] Leah M. Hunter,[1,2] Swati Keshri,[1,3] Ceri A. Fielding,[4] Katie Nightingale,[1,2] Benjamin Ravenhill,[1,2] Luis Nobre,[1,2] Martin Potts,[1,2] Robin Antrobus,[1,2] Colin M. Crump,[5] David C. Rubinsztein,[1,3] Richard J. Stanton,[4,7] and Michael P. Weekes[1,7,8,*]

[1]Cambridge Institute for Medical Research, University of Cambridge, Hills Road, Cambridge CB2 0XY, UK
[2]Department of Medicine, University of Cambridge, Hills Road, Cambridge CB2 2QQ, UK
[3]UK Dementia Institute, University of Cambridge, The Keith Peters Building, Hills Road, Cambridge CB2 0XY, UK
[4]Cardiff University School of Medicine, Division of Infection and Immunity, Henry Wellcome Building, Heath Park, Cardiff CF14 4XN, UK
[5]Division of Virology, Department of Pathology, University of Cambridge, Cambridge, UK
[6]These authors contributed equally
[7]Senior author
[8]Lead contact
*Correspondence: mpw1001@cam.ac.uk
https://doi.org/10.1016/j.chom.2024.02.013

SUMMARY

Human cytomegalovirus (HCMV) is an important human pathogen that regulates host immunity and hijacks host compartments, including lysosomes, to assemble virions. We combined a quantitative proteomic analysis of HCMV infection with a database of proteins involved in vacuolar acidification, revealing Dmx-like protein-1 (DMXL1) as the only protein that acidifies vacuoles yet is degraded by HCMV. Systematic comparison of viral deletion mutants reveals the uncharacterized 7 kDa US33A protein as necessary and sufficient for DMXL1 degradation, which occurs via recruitment of the E3 ubiquitin ligase Kip1 ubiquitination-promoting complex (KPC). US33A-mediated DMXL1 degradation inhibits lysosome acidification and autophagic cargo degradation. Formation of the virion assembly compartment, which requires lysosomes, occurs significantly later with US33A-expressing virus infection, with reduced viral replication. These data thus identify a viral strategy for cellular remodeling, with the potential to employ US33A in therapies for viral infection or rheumatic conditions, in which inhibition of lysosome acidification can attenuate disease.

INTRODUCTION

Human cytomegalovirus (HCMV) is a ubiquitous herpesvirus that persistently infects more than 60% of all people worldwide.[1] Reactivation of HCMV from latency in immunocompromised people including organ transplant recipients can cause significant morbidity and mortality.[2,3] HCMV is also a leading cause of congenital disease, affecting 0.5%–4% of pregnancies.[4] Here, it can cause a spectrum of disease including sensorineural deafness, intellectual disability, and microcephaly.[4] However, only four anti-HCMV drugs have been approved, all with significant toxicity and problematic drug resistance.[5]

As a virus that persists lifelong, and that has co-evolved with its human host over millions of years, HCMV is regarded as a master cellular regulator, systemically modulating multiple processes critical to infection. We previously found that >900 host proteins are downregulated >3-fold over the course of infection, with at least 163 proteins degraded in the proteasome or lysosome.[6–8] These studies highlighted previously unrecognized facets of innate immunity, including that helicase-like transcription factor (HLTF) and Schlafen family member 11 (SLFN11) are novel antiviral restriction factors targeted by the viral UL145 and RL1 proteins, respectively, and that mixed lineage kinase domain-like protein (MLKL) is degraded by HCMV UL36 to inhibit necroptotic cell death.[7–9] Small molecules that inhibit these and other HCMV-host interactions may offer novel therapeutic potential.[10]

During productive infection *in vitro*, expression of HCMV genes is conventionally divided into immediate-early, early, and late phases during a ~72–96 h lytic replication cycle.[11] We previously characterized five temporal classes of viral protein expression, offering finer definition of protein expression profiles.[7] Late during infection, HCMV hijacks host intracellular compartments (vacuoles) to facilitate viral replication, especially virion assembly and egress. For example, in fibroblasts, HCMV reorganizes the cytoskeleton and endocytic pathway to form virion assembly compartments (vACs), which contain virions and early endosomes in the core, and late endosomes/lysosomes at the periphery.[12,13] HCMV forms similar structures in endothelial cells, containing lysosomes and autophagosomes, but not early endosomes.[14] These studies suggest that lysosomes are necessary to assemble the HCMV virion. Lysosomes are also required during viral replication to degrade a variety of

CellPress
OPEN ACCESS

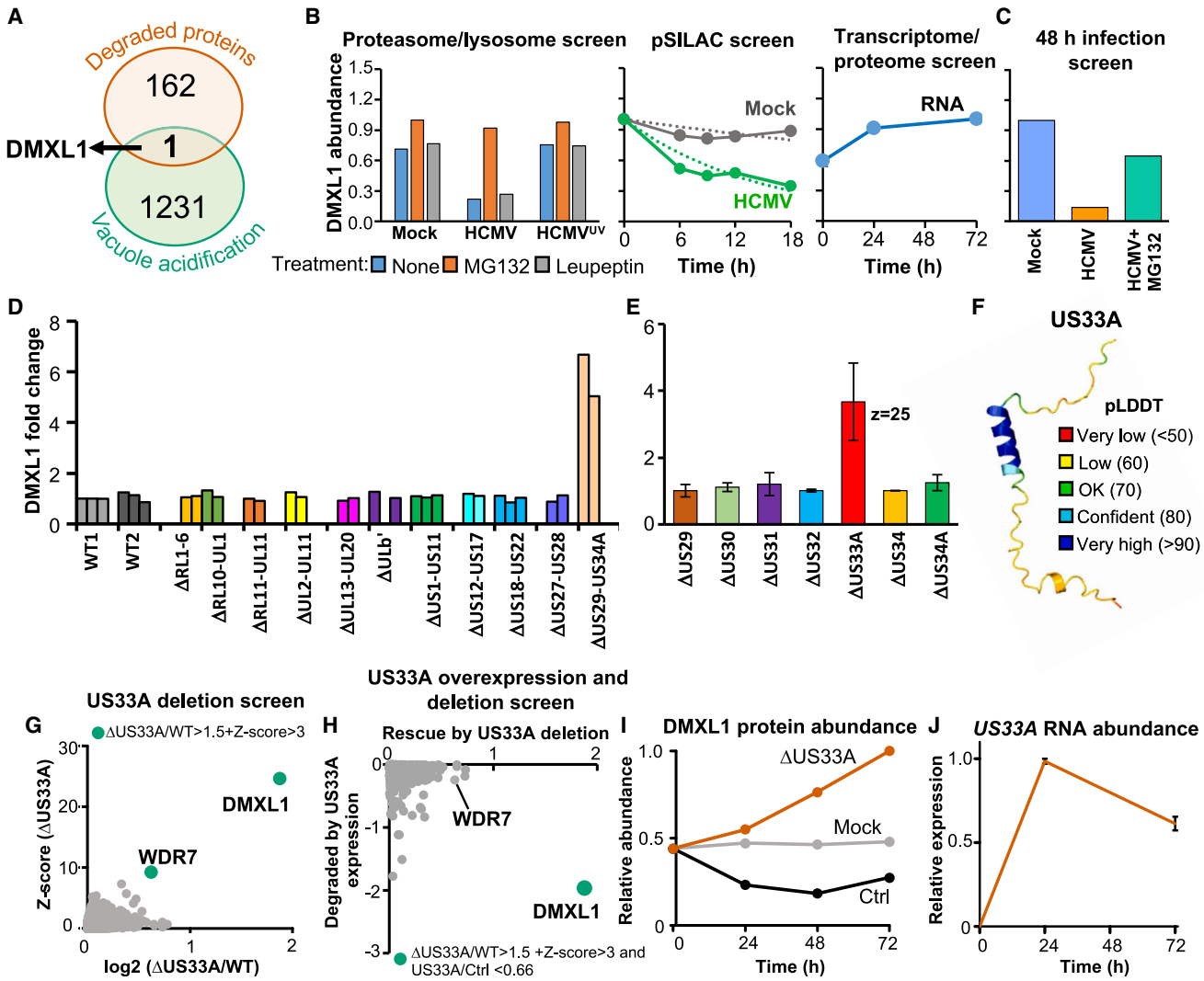

Figure 1. DMXL1 is targeted for degradation in the proteasome by HCMV US33A

(A) Venn diagram showing the overlap between 163 proteins that we previously identified to be degraded during early and/or late HCMV infection, with a database of 1,232 proteins that have roles in vacuolar acidification, from AmiGo (accession: GO: 0007035).[24]

The following three figures (B)–(D) are based on data from prior publications[7,8] and, along with data shown later in Figure 4A, are the only previously published data in this manuscript.

(B) Three orthogonal protein degradation screens showing that DMXL1 is degraded with high confidence during early HCMV infection, from Nightingale et al.[7] Left panel: DMXL1 was rescued from degradation by the proteasome inhibitor MG132 in HCMV-infected cells, but not during mock infection, infection with UV-irradiated HCMV ($HCMV^{UV}$), or inhibition with the lysosomal protease inhibitor leupeptin (see also Figure 1 from Nightingale et al.[7]). Middle panel: increased rate of DMXL1 degradation during HCMV compared with mock infection. Cells were pre-labeled with medium SILAC (stable isotope labelling by amino acids in cell culture) amino acids prior to infection, then switched to heavy amino acids at the point of infection. Quantification of medium-labeled proteins over time using TMT-based multiplexing facilitated quantification of protein degradation rates (see also Figure 2 from Nightingale et al.[7]). Right panel: relative abundance of DMXL1 transcript over 72 h infection. Although DMXL1 protein was not identified in this screen to enable simultaneous quantitation, DMXL1 was downregulated in our other experiments over a comparable time course suggesting that it is degraded (left panels and C; see also Figure 3 from Nightingale et al.[7]).

(C) DMXL1 is degraded during late HCMV infection (data from Fletcher-Etherington et al.[8]). The y axis scale is the same as (B).

(D) A proteomic screen of viral block deletion mutants determined that the US29-34A gene block is required to downregulate DMXL1. Bars of same color represent biological replicates, and all viruses were examined in duplicate or triplicate across three independent experiments (data from Nightingale et al.[9]). Fold change was calculated in comparison with strain Merlin wild-type 1 (WT1) control. A second control was included, comprising WT1 that lacked UL16 and UL18 genes.[7] Strain AD169 HCMV was used as the $\Delta U_L/b'$ strain in this study, and we confirmed that AD169 as well as Merlin-strain HCMV downregulates DMXL1 (Figure S2B).

(E) A proteomic screen of viral single-gene-deletion mutants determined that US33A is necessary for downregulation of DMXL1 (each virus was used at MOI = 7.5, n = 2, 60 h infection). Fold change (FC) was calculated from the average signal:noise for both ΔUS33 biological replicates divided by the average signal:noise for both control replicates. The *Z* score was calculated as described in Figure S1. See also Table S3.

(F) An AlphaFold model of US33A suggested that the protein is chiefly unstructured, with a central alpha helix (see Figure S2A for all models generated).

(legend continued on next page)

molecules important in innate and adaptive immunity.[15–20] In comparison with the cytoplasm and other intracellular vesicles with a neutral pH, lysosomes are acidic (pH 4.5–5), requiring the host V-ATPase to pump protons into the lumen.[21] Although the impact of lysosomal pH on viral replication is poorly defined, vacuolar acidification conducted by the ATP6V0C subunit of the V-ATPase may be necessary for vAC formation.[22]

To determine how HCMV may globally modulate lysosome function, we combined our proteomic analyses with a database of proteins involved in vacuolar acidification. Dmx-like protein-1 (DMXL1) was the only protein that acidifies vacuoles (via interaction with the V-ATPase[23]) and is also degraded by HCMV. We characterize the function of each of seven viral genes from a genetic block we identify as necessary to target DMXL1, determining that the previously uncharacterized HCMV US33A protein degrades DMXL1 by recruiting the Kip1 complex (KPC) E3 ligase. HCMV-induced DMXL1 degradation was sufficient to inhibit lysosomal acidification, autophagic cargo degradation, and vAC formation, all previously unidentified functions for viral proteins.

RESULTS

DMXL1 stimulates vacuolar acidification but is targeted for degradation by HCMV US33A

To identify host factors with roles in lysosomal acidification that are antagonized by HCMV, we overlapped data from our previous publications in which we identified proteins degraded early[7] and/or late[9] during HCMV infection with a database of proteins that regulate acidification of the vacuole.[24] Only DMXL1 fulfilled both criteria (Figures 1A–1C), suggesting that this protein may be of substantial importance both to the cell and to virus. DMXL1 has only been characterized in three prior publications, which identified that the 338 kDa protein is highly conserved with multiple WD40 repeats that fold to form β-propellers.[23,25,26] DMXL1 and DMXL2 interact with WD-repeat-containing protein 7 (WDR7) to form the complex Rabconnectin-3, which interacts with the V-ATPase in mouse kidney lysates.[23,27,28] The DMXL proteins are partially homologous to regulator of V-ATPase in vacuolar membrane protein 1 (RAV1), a component of the yeast regulator of H^+-ATPase of vacuolar and endosomal membranes (RAVE) complex, which is involved in the reassembly of dissociated V-ATPase V1 and V0 sectors.[29] In addition to a potential role in the control of V-ATPase trafficking, the DMXL proteins may play analogous roles to RAV1 in the assembly of V-ATPase subunits via WD40 domain interactions and are thought to promote intracellular vesicle acidification.[23,26,27]

To study whether HCMV regulates lysosomal acidification via DMXL1, we first needed to identify which of the 171 HCMV genes is involved. We previously conducted a proteomic screen using a panel of recombinant viruses deleted for one or other of a series of blocks of genes non-essential for viral replication *in vitro*.[9] This identified that DMXL1 is targeted by the uncharacterized viral *US29-US34A* block (Figure 1D). To determine which gene(s) in this block is required, we generated a library of HCMV single-gene deletion mutants in *US29-US34A* and infected telomerase reverse transcriptase-immortalized primary human fetal foreskin fibroblasts (HFFFs-TERTs) with these or the wild-type (WT) strain (Figure S1A). Multiplexed proteomic analysis of cellular lysates using tandem mass tag (TMT) peptide labels and MS3 mass spectrometry quantified 7,687 human and 158 viral proteins, revealing a diversity of functions for this gene block. These included regulation of innate immunity via inhibition of multiple interferon-stimulated genes by US30 and US34A; regulation of proteins involved in mitotic cell division by US31 and regulation of protein involved in secretion by US34 (Figure S1B; Tables S1 and S2). Data from proteomic experiments in this study are shown in Table S3. Here, the worksheet ''Plots'' is interactive, enabling generation of graphs of protein expression of any of the human and viral proteins quantified.

DMXL1 expression was only rescued by deletion of US33A, a small 7-kDa protein with a single predicted α-helix (Figures 1E, 1F, S1, and S2A). DMXL1 and the related WDR7 protein were the only proteins significantly upregulated after 72 h infection with ΔUS33A HCMV in comparison with WT virus (Figures 1G, S1B, and S3A). Overlap of these data with a complementary proteomic screen comparing stably overexpressed US33A with control suggested that this protein is both necessary and sufficient for DMXL1 downregulation. Furthermore, the combination of both screens suggested that DMXL1 and to a lesser extent WDR7 are the only bona fide targets of US33A (Figures 1H and S3B; Table S1). However, addition of either an N- or C-terminal tag ablated US33A-mediated DMXL1 degradation (Figures S3C and S3D), leading us to use untagged US33A for subsequent functional experiments. We did not detect any US33A peptides either in this study or previously using mass spectrometry, likely reflecting its small size and a paucity of peptides suitable for proteomic analysis. However, *US33A* transcript was detected within the first 24 h of HCMV infection, consistent with the kinetics of DMXL1 degradation (Figures 1I and 1J).

DMXL degradation by US33A disrupts lysosomal acidification

To determine whether degradation of DMXL1 by US33A inhibits lysosomal acidification, HFFF-TERTs stably expressing US33A or control were stained with LysoTracker DND 99. US33A expression reduced LysoTracker staining, indicative of a less acidic lysosome (Figure 2A). These findings were confirmed using the pH-sensitive probe LysoSensor yellow/blue (Figure 2B). Whereas LysoTracker quantitation is dependent on the total cellular LysoTracker signal, ratiometric quantification of LysoSensor staining at two different wavelengths minimizes the potential for error due to differences in dye uptake by

(G) Scatterplot of human proteins from (E) with Z > 0 and FC > 1 identified that DMXL1 and WDR7 significantly increase in abundance upon infection with ΔUS33A compared with WT HCMV.
(H) Overlap of data from (G) with a complementary proteomic screen comparing protein abundance in cells stably overexpressing US33A or a control vector, which quantified 7,687 proteins (see also Figures S3A–S3D).
(I) Proteomic quantitation of the relative abundance of DMXL1 over 72 h of infection as indicated (MOI = 5). 7,994 human and 143 viral proteins were quantified. See also Table S3.
(J) Quantification of US33A transcript over 24 h of infection at MOI = 10 by RT-qPCR. Error bars show standard error of the mean (SEM) for three replicates.

CellPress
OPEN ACCESS

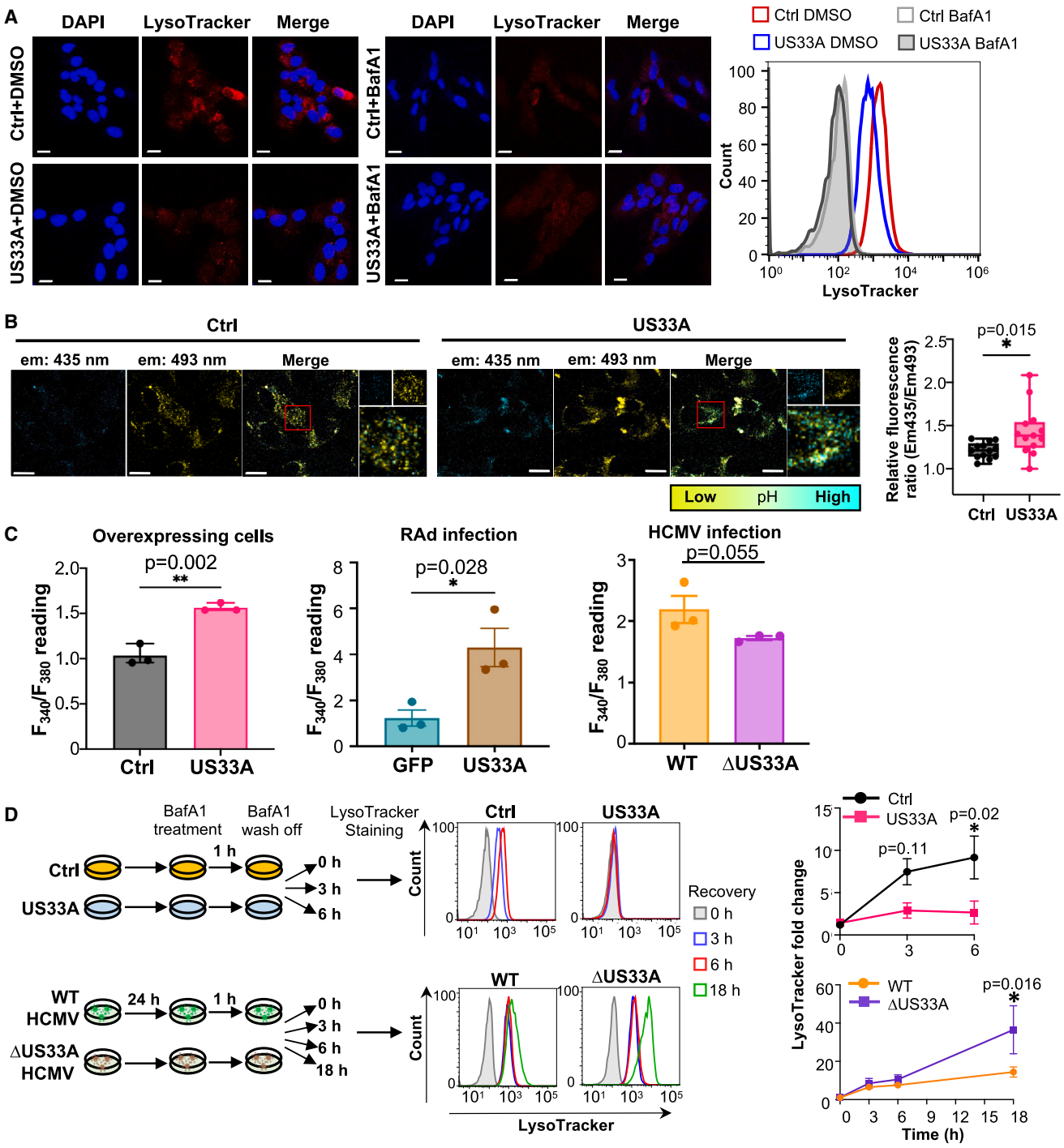

Figure 2. US33A reduces lysosomal acidification and impairs lysosomal pH maintenance

(A) LysoTracker DND-99 staining of lysosomes in HFFF-TERTs expressing US33A or a control vector. BafA1 treatment was at 400 nM for 4 h and LysoTracker at 1 μM for 30 min. Left: representative images. Scale bars: 20 μm. Right: representative flow cytometry results.

(B) LysoSensor yellow/blue DND-160 staining of lysosomes in HFFF-TERTs expressing US33A or a control vector. Scale bars: 10 μm. To measure fluorescence of LysoSensor in both confirmations using live-cell imaging, paired excitation/emission wavelengths 405/435 and 458/493 nm were employed as per previously published protocols.[30,31] Ten images with >10 cells per image were quantified. The box and whisker plot shows mean and range of the 435/493 emission ratio. The p value for a difference between control and US33A-expressing cells was estimated using an unpaired two-tailed t test. *p < 0.05.

(C) Quantification of LysoSensor staining using a microplate reader with excitation at 340 or 380 nm and emission at 527 nm as per previous protocols.[31,32] Staining with LysoSensor was at 5 μM for 10 min. Left panel: HFFF-TERTs expressing US33A or a control vector. Middle panel: HFFF-TERTs expressing the

(legend continued on next page)

each stained cell.[30] US33A-mediated impairment of lysosomal acidification was confirmed in HFFF-TERTs stably expressing US33A or control, infected with adenoviruses expressing US33A (RAd-US33A) or control and infected with WT or ΔUS33A HCMV (Figures 2C and S4A). Cells infected with RAd-US33A expressed a higher level of US33A mRNA, consistent with the increased magnitude of effect observed (Figure S3E).

A previous publication suggested that in mouse cells, knockdown of DMXL1 does not impact intravesicular acidification under baseline conditions; however, re-acidification of intracellular vesicles after bafilomycin A1 (BafA1) treatment is suppressed.[33] This indicated that cellular functions requiring significant and sustained upregulation of V-ATPase activity may be dependent on DMXL1. We designed experiments to recapitulate this phenotype with regard to US33A (Figure 2D). Lysosomes in HFFF-TERTs expressing US33A lost their ability to recover an acidic pH after 1 h BafA1 treatment. Infection of HFFF-TERTs with ΔUS33A HCMV enhanced lysosomal pH recovery after 1 h BafA1 treatment compared with WT HCMV-infected cells (Figure 2D). Small interfering RNA (siRNA) knockdown of DMXL1 phenocopied US33A expression and inhibited lysosomal pH recovery in HFFF-TERTs (Figures S4B and S4C). These results suggest that DMXL1 degradation by US33A causes functional lysosomal deficiency, which may be due to impaired V-ATPase regulation.

US33A inhibits autophagic cargo degradation

A functional V-ATPase and acidic lysosome are required for the terminal stages of autophagy: autophagosome-lysosome fusion and autophagosome degradation (Figure 3A).[34] To determine whether the lysosomal deficiency caused by US33A-mediated DMXL1 degradation impacts autophagy, we quantified LC3B-II. Accumulation of this classical marker of autophagosome abundance either indicates enhanced autophagosome formation or impaired autophagosome degradation.[35–37] To distinguish between these two possibilities, we also applied the V-ATPase inhibitor BafA1 to block autophagasome/LC3B-II degradation completely, meaning that measurement of LC3B-II would indicate autophagosome synthesis.[38,39] US33A expression in HFFF-TERTs via stable lentiviral transduction or adenoviral infection significantly enhanced LC3B-II accumulation in the absence, but not in the presence of BafA1 (Figures 3B, 3C, S5A, and S5B). These findings suggest that US33A leads to inhibition of autophagosome degradation. To recapitulate the experiment during HCMV infection, we used a high MOI = 25 to ensure infection of the greatest number of cells. Pre-incubation of HFFF-TERTs with serum-free medium can enable high-percentage infection at a lower MOI[8,20,40]; however, nutrient starvation can rapidly upregulate autophagic flux and autophagosome degradation,[41] which would confound data. In comparison with infection with WT HCMV, infection with ΔUS33A HCMV reduced LC3B-II accumulation in DMSO-treated cells but had no significant effect in BafA1-treated cells, which is consistent with US33A-mediated inhibition of autophagosome degradation (Figures 3D and S5C). siRNA knockdown of DMXL1 phenocopied US33A expression and inhibited LC3B-II degradation, suggesting that inhibition of autophagosome degradation by US33A is mediated by DMXL1 degradation (Figure S5D).

A reduction in autophagosome degradation might be caused by a decrease in autophagic cargo degradation due to reduced lysosome activity, impaired lysosomal-autophagosome fusion, or both.[30] To identify which applied here, co-localization between LC3B (autophagosome marker) and LAMP1/CD63 (lysosome/late endosome markers) was measured. Stable US33A expression enhanced co-localization of endogenous LC3B with LAMP1 and increased expression of both markers, suggesting that autophagosome-lysosome fusion was not impaired upon DMXL1 degradation and that LC3B-II degradation was likely to have been retarded, as we have previously observed in similar circumstances[30,42] (Figures 3E, 3F, and S5E; Video S1). Infection with ΔUS33A HCMV led to reduced LC3B-LAMP1 co-localization and expression in comparison with WT HCMV infection (Figures 3G, 3H, and S5F). These results suggest that US33A-mediated DMXL1 deficiency inhibits autophagosome degradation in lysosomes, rather than inhibiting the fusion between lysosomes and autophagosomes.

US33A degrades DMXL1 via recruitment of the KPC E3 ligase complex

We previously conducted a systematic interactome analysis of 169 canonical HCMV proteins, and a subset of non-canonical HCMV proteins, in infected cells.[40] Although this study purified complexes using C-terminal V5 tags, which ablate US33A-mediated DMXL1 degradation (Figure S3C), it was nevertheless possible that US33A retained the ability to recruit the relevant DMXL1 degradation machinery. Interactome analysis revealed that US33A-V5 interacts with RNF123 and UBAC1, the catalytic and non-catalytic subunits of the KPC E3 ligase (Figure 4A). We confirmed the interaction between US33A and RNF123/UBAC1 by co-immunoprecipitation (coIP) (Figures 4B and S6A) and, using a series of US33A deletion or truncation mutants, determined that the US33A N terminus is necessary to recruit KPC (Figures 4C and S6B).

To determine whether KPC is required for US33A to degrade DMXL1, CRISPR-Cas9 was used to knock out RNF123, UBAC1, or both in HFFF-TERTs, followed by infection with WT or ΔUS33A HCMV. In all three knockout cell types, DMXL1 was rescued during WT HCMV infection to a level similar to that during ΔUS33A infection (Figures 4D and S6C; Table S4), indicating that US33A degrades DMXL1 via recruitment of KPC.

US33A delays the formation of the virion assembly compartment and negatively regulates the replication of HCMV and HSV-1

To determine whether the effects of US33A on lysosomal pH and autophagy may modulate viral assembly compartment (vAC)

coxsackie virus and adenovirus receptor (HFFF-CARs) infected with adenovirus expressing US33A or GFP (MOI 5 for 72 h). Right panel: HFFF-TERTs infected with WT or ΔUS33A HCMV (MOI 5 for 24 h). Values shown are mean ± SEM (n = 3 independent experiments; each value was calculated from the mean of five technical replicates).

(D) US33A inhibits lysosomal re-acidification. Left panels: schematics of workflow. Right panels: quantification of lysosomal acidity via LysoTracker staining in HFFF-TERTs expressing US33A or a control vector (top; 400 nM BafA1 for 1 h) or infected with parental or ΔUS33A HCMV (bottom; 100 nM BafA1 for 1 h). Values shown are mean ± SEM (n = 3 independent experiments). p values were estimated using an unpaired two-tailed t test. *$p < 0.05$.

CellPress
OPEN ACCESS

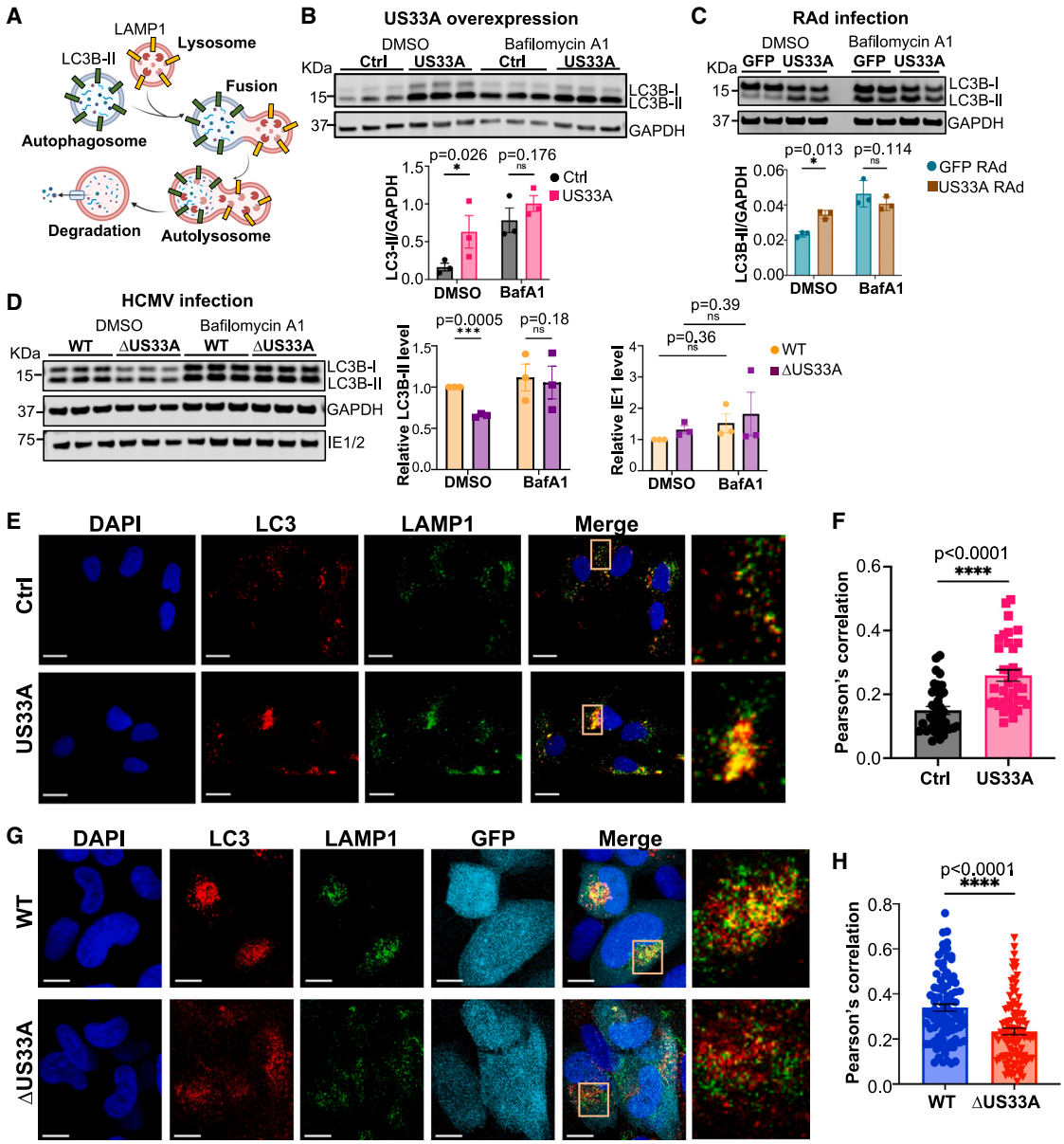

Figure 3. Autophagic cargo degradation is inhibited by US33A

(A) Schematic of the autophagy pathway after the formation of autophagosomes.

(B–D) LC3B-II expression in (B) HFFF-TERTs stably expressing US33A or control; (C) HFFF-CARs infected with adenovirus expressing US33A or GFP at MOI 5 for 72 h, or (D) HFFF-TERTs infected with WT or ΔUS33A HCMV at MOI 25 for 48 h. Cells were treated with vehicle (DMSO) or BafA1 at 400 nM for 4 h, as indicated. Left panels: immunoblots of LC3B. Right panels: quantification of ratios of LC3B-II:GAPDH. Error bars show SEM for three independent experiments. p values were estimated using two-way ANOVA. *$p < 0.05$, ***$p < 0.001$, ns, not significant, $p > 0.05$. For (D), for each experiment, LC3B-II/GAPDH (middle panel) or IE1/GAPDH ratios (right panel) were first normalized to the ratio of DMSO-treated WT HCMV prior to calculating mean values.

(E) Co-localization of LC3B and LAMP1 in HFFF-TERTs stably expressing US33A or a control vector, by immunofluorescence. Scale bars: 20 μm.

(F) Quantification of (E), using >10 cells from each of a total of 36 images from three independent experiments.

(G) Co-localization of LC3B and LAMP1 in HFFF-TERTs infected with WT or ΔUS33A HCMV at MOI 0.5 for 24 h. GFP fluorescence was used to identify infected cells. Scale bars: 10 μm.

(H) Quantification of (G), 93 WT HCMV and 97 ΔUS33A infected cells from over 30 images from three independent experiments. Pearson's correlation was used for (F) and (H), with p values estimated using unpaired two-tailed t tests: ****$p < 0.0001$. Full data quantifying Pearson's correlation are shown in Table S5.

formation, we performed a temporal analysis during infection with WT and ΔUS33A HCMV. Mature vACs were identified as a juxtanuclear structure formed by a ring of giantin, a marker for the Golgi body, outside a core of the HCMV envelope glycoprotein B (gB)[12,43–47] (Figures 4E and S7A). Early/immature vACs were identified as infected cells expressing gB but without ring-shaped giantin.[12,45] vACs formed significantly earlier in cells infected with ΔUS33A HCMV compared with WT (Figures 4E and

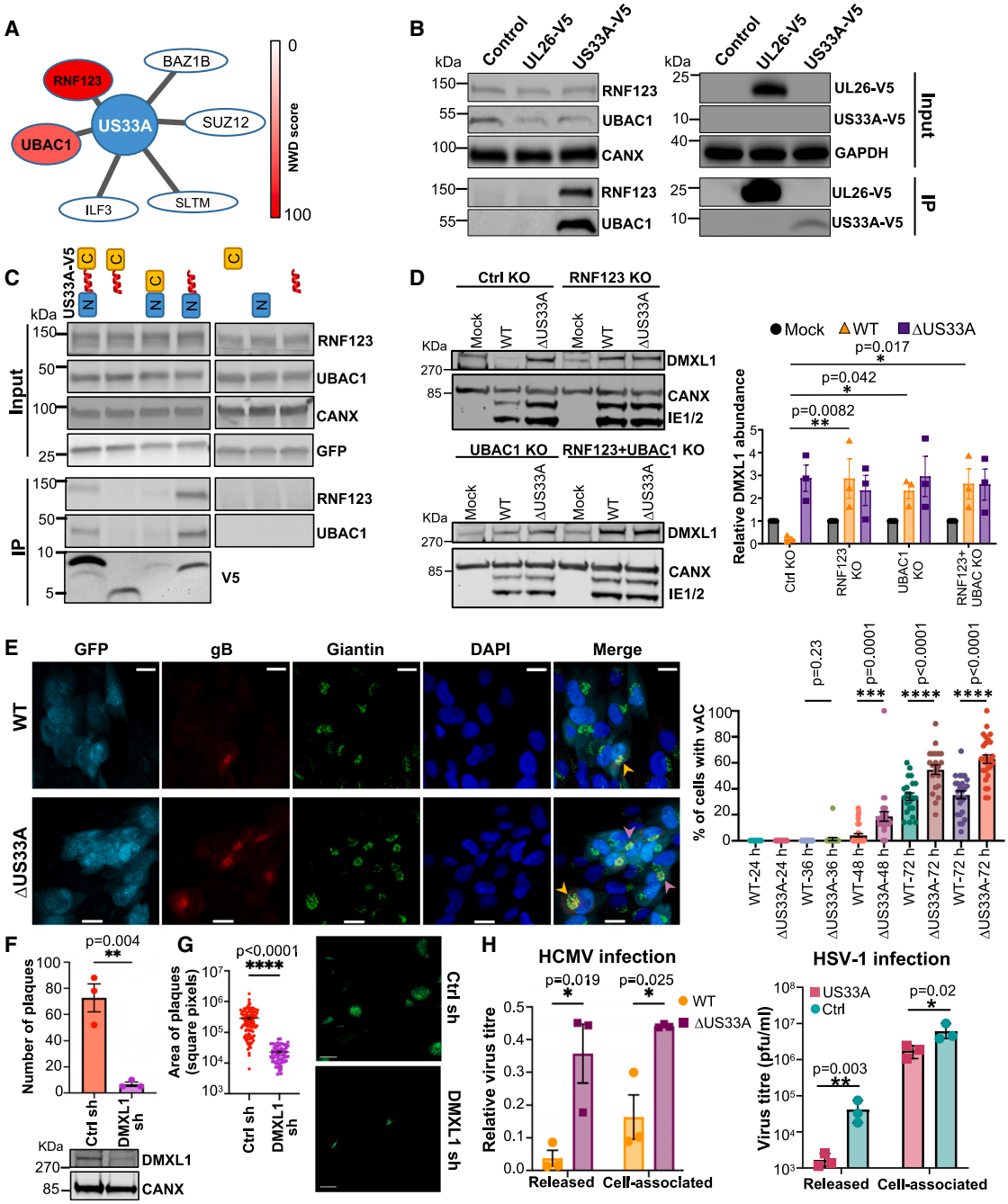

Figure 4. HCMV US33A recruits the KPC E3 ligase to degrade DMXL1 and inhibit vAC formation

(A) High-confidence interacting proteins for US33A from our previous systematic interactome analysis of all canonical HCMV genes in infected cells (data from Nobre et al.[40]). The normalised weighted *D* (NWD) score is calculated from the fraction of runs in which an interacting protein is observed, the number of peptides from this protein and the standard deviation of this number across all IPs, and the reproducibility of detection across US33A replicates.

(B) CoIP validating that US33A interacts with RNF123 and UBAC1.

(C) CoIP showing that the US33A N terminus is necessary to recruit RNF123 and UBAC1. Expression of the N terminus, alpha helix, and C-terminal regions of US33A-V5 in isolation was validated by qPCR as the proteins were of insufficient size to detect by immunoblot (Figure S6B).

(D) HCMV US33A downregulates DMXL1 in a KPC-dependent manner. Polyclonal bulk populations of HFFF-TERTs edited using CRISPR-Cas9 as indicated were infected with WT or ΔUS33A HCMV at MOI 5 for 72 h. The left panel shows a representative immunoblot from two independent experiments. Blotting for HCMV IE1/2 confirmed similar infection in each cell type. Immunoblots for RNF123 and UBAC1 are shown in Figure S6C. The right panel shows the quantification of DMXL1 for three independent experiments (error bars: mean ± SEM). p values were estimated using two-way ANOVA, *p < 0.05, **p < 0.01.

(legend continued on next page)

S7–S9), suggesting that vAC formation may depend either on vacuolar pH, autophagy, or both and that this is delayed in the absence of DMXL1. To determine whether US33A delays vAC formation by modulating vacuolar pH, we infected HFFF-TERTs with WT or ΔUS33A HCMV in the presence of BafA1. BafA1 significantly delayed the formation of vACs at 48 h post-infection (hpi) in ΔUS33A HCMV-infected cells with a similar but non-significant trend in WT-infected cells and completely inhibited vAC formation with both WT and ΔUS33A HCMV infection at 72 h (Figure S9). This provides a mechanistic link between US33A-mediated inhibition of lysosomal acidification/autophagosome degradation and delayed vAC formation.

To determine whether US33A-mediated effects on vAC formation are reflected in viral replication, we quantified the number and size of plaques formed in DMXL1 shRNA (short hairpin RNA) knockdown cells compared with control (Figures 4F and 4G). As Merlin-strain viruses are recognized to plaque inefficiently,[48] for this experiment, strain AD169-GFP was employed.[15] Knockdown of DMXL1 inhibited both the number and size of plaques. To determine whether DMXL1 degradation by US33A also inhibits viral replication, HFFF-TERTs were infected with the same WT or ΔUS33A Merlin-strain HCMV as used in all of our other experiments at MOI = 0.1 for 6 days, to facilitate approximately two viral replication cycles. Infection with ΔUS33A HCMV significantly increased both cell-associated and released viral titers compared with WT infection (Figure 4H), indicating that US33A negatively regulates HCMV replication. Furthermore, infection with ΔUS33A HCMV did not significantly increase viral release compared with WT in cells knocked down for DMXL1 using siRNA, highlighting the relevance of DMXL1 as US33A's target (Figure S10C). The greater effect of DMXL1 KD on viral release compared with infection with WT (US33A-expressing) virus likely reflects (1) more complete abrogation of DMXL1 expression by siRNA compared with infection with a US33A-expressing virus and (2) knockdown of DMXL1 from the beginning of the viral replication cycle via siRNA compared with US33A-expression-dependent DMXL1 degradation. To determine whether US33A has a more general impact on other herpesviruses, we infected HFFF-TERTs expressing US33A or control with herpes simplex virus-1 (HSV-1), which shares a similar vAC-based viral replication strategy yet does not express a US33A homolog.[49] HSV-1 replication was also significantly inhibited in cells expressing US33A compared with control (Figure 4H).

DISCUSSION

Herpesviruses achieve lifelong persistence in infected individuals by utilizing a wide range of strategies to modulate cellular processes of the host. These include the deployment of proteins to target host factors for degradation. Degradation of DMXL1 by US33A and the KPC E3 ligase complex increases lysosomal pH, inhibits autophagy, and delays assembly of the vAC, reducing viral replication. US33A therefore functions to globally regulate cellular remodeling during infection. Functions were also ascribed to each of the other members of the previously uncharacterized HCMV US29-34A block of viral genes.

Only a few studies have hitherto examined manipulation of host lysosomes by HCMV. These have chiefly focused on subversion of lysosome function to degrade certain key molecules important in host innate or adaptive immunity, for example, major histocompatibility complex (MHC) class I polypeptide-related sequences (MIC) A/B, Toll-like receptor (TLR) 3/4, natural killer (NK) cell regulator B7-H6, human leukocyte antigen (HLA)-DR, and multidrug resistance-associated protein 1 (MRP1).[15–20] We previously systematically defined host proteins targeted for lysosomal degradation throughout the course of HCMV infection via application of the lysosomal protease inhibitor leupeptin.[7,20] However, there was no enrichment at any time point in the average abundance of these degraded proteins in cells infected with ΔUS33A virus compared with WT. Use of published data relating change in lysosomal pH to change in LysoSensor emission suggested that the pH difference between lysosomes from cells infected with WT HCMV or ΔUS33A HCMV was ~0.3.[50,51] This relatively modest change may be insufficient to modulate lysosomal degradation, yet sufficient to modify autophagy and vAC formation.

Although no other HCMV proteins are known to modulate lysosome function, a systematic microRNA screen demonstrated that HCMV miR-US25-1 targets the ATP6V0C transcript, which encodes an essential component of the lysosomal V-ATPase. siRNA knockdown of ATP6V0C reduced replication of the highly-passaged laboratory HCMV strain AD169.[22,52] It remains to be determined whether virally expressed miR-US25-1 reproduces

(E) vAC formation time course, see Figure S7 for full data. Cells were infected with WT or ΔUS33A HCMV at MOI 1. At 24 h post-infection (hpi), both viruses infected a similar proportion of cells (Figure S7B). Left panel: representative images at 48 hpi. Pink arrows: examples of mature vACs. Orange arrows: examples of early/immature vACs. These were counted separately for the purpose of quantification (Figures S7C and S9C). Scale bars: 20 μm. Right panel: percentage of infected cells with mature vACs at each time point. Similar results were observed in a second independent experiment (Figure S8). The number of images with infected cells assessed at each time point were: 24 h (n = 21 images with 112 infected cells for WT; n = 22, 115 for ΔUS33A); 36 h (n = 31, 122 for WT; n = 21, 146 for ΔUS33A); 48 h (n = 21, 240 for WT, n = 27, 241 for ΔUS33A); 72 h (n = 22, 205 for WT, n = 21, 188 for ΔUS33A); 96 h (n = 25, 389 for WT, n = 27, 321 for ΔUS33A). p values were estimated using a two-tailed unpaired t test. ***$p < 0.001$, ****$p < 0.0001$.

(F) Top panel: number of plaques (defined as a group of >5 cells) formed by AD169-GFP in HFFF-TERTs treated with DMXL1 or control shRNA. AD169 degrades DMXL1 similarly to WT Merlin strain, as shown in Figures 1D and S2B. Error bars show SEM of three independent experiments. **$p < 0.01$ (unpaired two-tailed t test). Bottom panel: immunoblot showing DMXL1 knockdown efficiency by shRNA. We confirmed that US33A expression was not affected by DMXL1 shRNAs (Figures S10A and S10B).

(G) Left panel: quantification of the plaque size from the experiment described in (F). Error bars show SEM for >60 plaques. ****$p < 0.0001$ (unpaired two-tailed t test). Right panel: representative images of plaque morphology. Scale bars: 1 mm.

(H) Left panel: relative titers of released and cell-associated WT or ΔUS33A HCMV after 6 days of infection at MOI 0.1. Because absolute titers varied from experiment to experiment, relative titers were calculated for each experiment and then averaged between experiments (see STAR Methods). Right panel: titer of released and cell-associated herpes simplex virus-1 (HSV-1) in HFFF-TERTs expressing US33A or control after 24 h of infection at MOI 0.1. Error bars show SEM for three independent experiments. p values were estimated using unpaired two-tailed t tests. *$p < 0.05$, **$p < 0.01$.

this phenotype, reduces lysosomal acidification, and inhibits autophagy, as might be expected from our present study. If so, this would suggest that HCMV encodes two complementary strategies to achieve the same aim and that the virus is willing to sacrifice replication efficiency to facilitate its overall lifecycle. Assuming DMXL1 is also downregulated in other cell types infected with HCMV *in vitro*, possible explanations might include (1) immune evasion (for example, in dendritic cells), since endosomal acidification is required for efficient MHC class II presentation and efficient signaling by TLRs[53,54]; (2) promotion of latent infection by inhibition of viral assembly in monocytes or other latent reservoirs[55]; or (3) prevention of excessive viral replication, tissue destruction, and inflammation whose overall effects might affect the balance between immune control and viral clearance, or change the duration of transmission from host-to-host. Prior studies in which HCMV was systematically mutagenized identified other temperance factors that also reduce viral replication including RL13, UL9, and US30,[56,57]; however, none have hitherto been mechanistically characterized. US33A was not included in these studies, having only been identified in 2011.[58]

A systems-based analysis of HCMV-induced organelle remodeling revealed that during late infection, lysosomes are distributed into two distinct populations.[59] The first, denser fraction, was found in discrete punctate structures and was defined by expression of molecules involved in carbohydrate catabolism such as lysosomal alpha-glucosides. The second, less-dense LAMP1-positive fraction localized to the vAC.[59] Our data suggest that this latter population may play important roles with regard to US33A function, given the co-localization we observed between LAMP1 and LC3B in ΔUS33A HCMV-infected cells.

The impact of HCMV infection on autophagy remains incompletely defined and varies according to the stage of viral replication.[60] Autophagy is promoted early during infection via increased lipidation of LC3-I into LC3-II and increased generation of autophagosomes.[61,62] By 24 h, expression of HCMV TRS1 and IRS1 block the first stages of autophagy by targeting the Beclin 1 complex, a key regulator of phagophore and autophagosome formation.[61,63] US33A may thus complement IRS1/TRS1 function by blocking the last stages of autophagy, namely autophagic cargo degradation. The impact of autophagy on HCMV replication also remains incompletely defined, and conflicting phenotypes have been described. A proviral role has been suggested by recent studies that have either employed knockdown of autophagy components or chemical modulators.[47,61] Our data support these observations, relating inhibited autophagy during US33A expression to reduced viral replication.

The overall effect of US33A is somewhat paradoxically to delay vAC formation and diminish viral replication. Reduced autophagic cargo degradation might have been expected to increase availability of membrane for forming HCMV particles, and a more alkaline lysosome might have been expected to degrade new HCMV particles to a lesser degree. However, the key factor that determines viral replication efficiency might be pH in the endosome/lysosome/vAC, with a more acidic vacuole promoting vAC formation. As discussed above, earlier vAC formation in the absence of US33A might present an overall disadvantage to the viral lifecycle, for example, by facilitating viral antigen presentation at a stage of replication in which adaptive immune evasion is critical.

The power of our prior HCMV interactome analysis to reveal viral mechanism is exemplified by our identification that the KPC complex is required for DMXL1 degradation. Given that this study identified interactions between 51 HCMV proteins and E3 ligases,[40] additional insights are likely to result for other proteins degraded by HCMV that so far remain mechanistically uncharacterized. The lack of an observed direct interaction between US33A and DMXL1 is most likely to reflect the effect of the V5 tag, which in this study completely ablated DMXL1 degradation when applied either at US33A's N or C terminus. Given our demonstration of the interaction between US33A's N terminus and the KPC complex, it is plausible that the US33A C terminus may interact with DMXL1. Further analyses will require generation of an antibody specific for unmodified US33A. Functionally, the 57 amino acid US33A is most likely to act in a manner akin to a viral proteolysis-targeting chimera (PROTAC), linking KPC together with DMXL1 to facilitate its degradation.[64]

US33A is conserved across 264 strains of HCMV with several minor mutations and in chimpanzee cytomegalovirus (CCMV), which is the closest relative of HCMV (Figure S11A; Data S1). However, no homologs are found in other primate cytomegaloviruses, or other betaherpesviruses such as human herpesvirus-6 and -7 (HHV-6 and HHV-7). The divergence of HCMV from HHV-6 and HHV-7 occurred prior to the branching of cytomegaloviruses into species-specific lineages (Figure S11B), suggesting that the acquisition of US33A by HCMV and CCMV occurred during transmission between great apes in the past few million years.[65–68]

As US33A is not conserved in any other human pathogen and is a small protein, an intriguing possibility is its potential use as a therapeutic agent. In addition to herpesviruses, multiple viruses require an acidic endosome at one or other point during their replication cycle. For example, cellular entry of RNA viruses including severe acute respiratory syndrome coronavirus 2 (SARS-CoV-2), influenza A, and human rhinoviruses is highly dependent on endosomal pH.[69–72] Replication of *Alphaviruses* such as Sindbis virus also requires acidic endosomes.[73] Although it is unclear at present whether the relatively modest change in lysosomal pH offered by US33A-mediated DMXL1 degradation will be sufficient to inhibit these processes, smaller changes in endosomal pH may result in fewer toxic effects, than for strong protein flux inhibitors such as BafA1.[74] Although HCMV entry into human fibroblasts is pH independent,[75–78] via fusion at plasma membrane, and we did not observe an effect of US33A expression on viral entry into retinal epithelial cells, in which entry is pH dependent[76] (Figure S10D), it is nevertheless possible that US33A may impair HCMV entry into other cell types in which entry is pH dependent, such as other epithelial cells or myeloid lineage cells. Chloroquine and hydroxychloroquine are lysosomotropic agents that raise intracellular pH, impair autophagic protein degradation, and are widely prescribed to patients with rheumatic diseases such as lupus and rheumatoid arthritis.[79,80] However, these drugs can exhibit off-target effects, for example, via interaction with TLR ligands and mitochondria, and toxicity remains a major limitation.[81–85] A more selective inhibitor of lysosomal acidification such as US33A might therefore be a worthy therapeutic candidate. Furthermore, over-acidification of lysosomes due to genetic deficiencies can lead to metabolic disorders, for example, mucopolysaccharidosis plus

(MPS+) and mucolipidosis IV (MLIV).[86–88] Here, the over-acidified environment within lysosomes may result in the malfunction of various lysosomal hydrolases, leading to a substrate accumulation, which might be ameliorated via US33A-based therapy. Finally, the scope of targeted PROTAC-based protein degradation will increase commensurate with an increased diversity of E3 ligases that can be hijacked. Modification of US33A to the minimal essential sequence that enables recruitment of KPC and chosen target(s) of interest may therefore provide a tool to this expanding armory.[64]

STAR★METHODS

Detailed methods are provided in the online version of this paper and include the following:

- KEY RESOURCES TABLE
- RESOURCE AVAILABILITY
  - Lead contact
  - Materials availability
  - Data and code availability
- EXPERIMENTAL MODEL AND SUBJECT DETAILS
  - Cells and cell culture
  - Viruses
- METHOD DETAILS
  - Viral infections
  - Plasmid construction
  - Stable cell line production
  - CRISPR/Cas9-mediated gene disruption
  - siRNA knockdown
  - Proteomic analyses
- QUANTIFICATION AND STATISTICAL ANALYSIS
  - Data analysis
  - Pathway analysis
  - Immunofluorescence microscopy analysis
  - AlphaFold2 prediction

SUPPLEMENTAL INFORMATION

Supplemental information can be found online at https://doi.org/10.1016/j.chom.2024.02.013.

ACKNOWLEDGMENTS

We are grateful to Prof. Steve Gygi for providing access to the "MassPike" software pipeline for quantitative proteomics. We are also grateful to the Cambridge Institute for Medical Research core facilities in flow cytometry and microscopy. This work was supported by Medical Research Council project grants (MR/X000516/1) to M.P.W. and (MR/S00971X/1) R.J.S. and a Royal Society University Research Fellowship (UF090010) and BBSRC grant (BB/M021424/1) to C.M.C. Funding was also received from the UK Dementia Research Institute (funded by the MRC, Alzheimer's Research UK, and the Alzheimer's Society), The Cambridge Commonwealth, European & International Trust (to S.K.), the Nehru Trust for Cambridge University and the Trinity-Henry Barlow Scholarship (to S.K.), and the NIHR Cambridge Biomedical Research Centre (NIHR203312). The views expressed are those of the authors and not necessarily those of the NIHR or the Department of Health and Social Care.

AUTHOR CONTRIBUTIONS

Conceptualization: M.P.W. Investigation: H.L., A.F.-E., L.M.H., S.K., C.A.F, K.N., B.R., L.N., R.A., and C.M.C. Data analysis: H.L., A.F.-E., K.N., and M.P.W. Funding acquisition: M.P.W. Supervision: D.C.R., R.J.S., and M.P.W. Writing: H.L., A.F.-E., and M.P.W. All authors edited the manuscript.

DECLARATION OF INTERESTS

D.C.R. is a consultant for Aladdin Healthcare Technologies Ltd., Mindrank AI, Nido Biosciences, Drishti Discoveries, Retro Biosciences and PAQ Therapeutics.

Received: August 2, 2023
Revised: January 10, 2024
Accepted: February 20, 2024
Published: March 12, 2024

REFERENCES

1. Zuhair, M., Smit, G.S.A., Wallis, G., Jabbar, F., Smith, C., Devleesschauwer, B., and Griffiths, P. (2019). Estimation of the worldwide seroprevalence of cytomegalovirus: A systematic review and meta-analysis. Rev. Med. Virol. *29*, e2034.
2. Reinke, P., Prösch, S., Kern, F., and Volk, H.D. (1999). Mechanisms of human cytomegalovirus (HCMV) (re)activation and its impact on organ transplant patients. Transpl. Infect. Dis. *1*, 157–164.
3. Nichols, W.G., Corey, L., Gooley, T., Davis, C., and Boeckh, M. (2002). High risk of death due to bacterial and fungal infection among cytomegalovirus (CMV)-seronegative recipients of stem cell transplants from seropositive donors: evidence for indirect effects of primary CMV infection. J. Infect. Dis. *185*, 273–282.
4. Buxmann, H., Hamprecht, K., Meyer-Wittkopf, M., and Friese, K. (2017). Primary Human Cytomegalovirus (HCMV) Infection in Pregnancy. Dtsch. Arztebl. Int. *114*, 45–52.
5. Tan, B.H. (2014). Cytomegalovirus Treatment. Curr. Treat. Options Infect. Dis. *6*, 256–270.
6. Weekes, M.P., Tomasec, P., Huttlin, E.L., Fielding, C.A., Nusinow, D., Stanton, R.J., Wang, E.C.Y., Aicheler, R., Murrell, I., Wilkinson, G.W.G., et al. (2014). Quantitative temporal viromics: an approach to investigate host-pathogen interaction. Cell *157*, 1460–1472.
7. Nightingale, K., Lin, K.M., Ravenhill, B.J., Davies, C., Nobre, L., Fielding, C.A., Ruckova, E., Fletcher-Etherington, A., Soday, L., Nichols, H., et al. (2018). High-Definition Analysis of Host Protein Stability during Human Cytomegalovirus Infection Reveals Antiviral Factors and Viral Evasion Mechanisms. Cell Host Microbe *24*, 447–460.e11.
8. Fletcher-Etherington, A., Nobre, L., Nightingale, K., Antrobus, R., Nichols, J., Davison, A.J., Stanton, R.J., and Weekes, M.P. (2020). Human cytomegalovirus protein pUL36: A dual cell death pathway inhibitor. Proc. Natl. Acad. Sci. USA *117*, 18771–18779.
9. Nightingale, K., Potts, M., Hunter, L.M., Fielding, C.A., Zerbe, C.M., Fletcher-Etherington, A., Nobre, L., Wang, E.C.Y., Strang, B.L., Houghton, J.W., et al. (2022). Human cytomegalovirus protein RL1 degrades the antiviral factor SLFN11 via recruitment of the CRL4 E3 ubiquitin ligase complex. Proc. Natl. Acad. Sci. USA *119*, e2108173119.
10. Nathans, R., Cao, H., Sharova, N., Ali, A., Sharkey, M., Stranska, R., Stevenson, M., and Rana, T.M. (2008). Small-molecule inhibition of HIV-1 Vif. Nat. Biotechnol. *26*, 1187–1192.
11. Mocarski, E.S., Shenk, T., and Pass, R.F. (2007). Cytomegaloviruses (Lippincott Williams & Wilkins).
12. Cepeda, V., Esteban, M., and Fraile-Ramos, A. (2010). Human cytomegalovirus final envelopment on membranes containing both trans-Golgi network and endosomal markers. Cell. Microbiol. *12*, 386–404.
13. Krzyzaniak, M.A., Mach, M., and Britt, W.J. (2009). HCMV-encoded glycoprotein M (UL100) interacts with Rab11 effector protein FIP4. Traffic *10*, 1439–1457.
14. Momtaz, S., Molina, B., Mlera, L., Goodrum, F., and Wilson, J.M. (2021). Cell type-specific biogenesis of novel vesicles containing viral products in human cytomegalovirus infection. J. Virol. *95*, e02358-20.

15. Fielding, C.A., Aicheler, R., Stanton, R.J., Wang, E.C., Han, S., Seirafian, S., Davies, J., McSharry, B.P., Weekes, M.P., Antrobus, P.R., et al. (2014). Two novel human cytomegalovirus NK cell evasion functions target MICA for lysosomal degradation. PLoS Pathog. *10*, e1004058.

16. Park, A., Ra, E.A., Lee, T.A., Choi, H.J., Lee, E., Kang, S., Seo, J.Y., Lee, S., and Park, B. (2019). HCMV-encoded US7 and US8 act as antagonists of innate immunity by distinctively targeting TLR-signaling pathways. Nat. Commun. *10*, 4670.

17. Weekes, M.P., Tan, S.Y., Poole, E., Talbot, S., Antrobus, R., Smith, D.L., Montag, C., Gygi, S.P., Sinclair, J.H., and Lehner, P.J. (2013). Latency-associated degradation of the MRP1 drug transporter during latent human cytomegalovirus infection. Science *340*, 199–202.

18. Charpak-Amikam, Y., Kubsch, T., Seidel, E., Oiknine-Djian, E., Cavaletto, N., Yamin, R., Schmiedel, D., Wolf, D., Gribaudo, G., Messerle, M., et al. (2017). Human cytomegalovirus escapes immune recognition by NK cells through the downregulation of B7-H6 by the viral genes US18 and US20. Sci. Rep. *7*, 8661.

19. Odeberg, J., Plachter, B., Brandén, L., and Söderberg-Nauclér, C. (2003). Human cytomegalovirus protein pp65 mediates accumulation of HLA-DR in lysosomes and destruction of the HLA-DR alpha-chain. Blood *101*, 4870–4877.

20. Fielding, C.A., Weekes, M.P., Nobre, L.V., Ruckova, E., Wilkie, G.S., Paulo, J.A., Chang, C., Suárez, N.M., Davies, J.A., Antrobus, R., et al. (2017). Control of immune ligands by members of a cytomegalovirus gene expansion suppresses natural killer cell activation. eLife *6*, e22206.

21. Mindell, J.A. (2012). Lysosomal acidification mechanisms. Annu. Rev. Physiol. *74*, 69–86.

22. Pavelin, J., McCormick, D., Chiweshe, S., Ramachandran, S., Lin, Y.T., and Grey, F. (2017). Cellular v-ATPase is required for virion assembly compartment formation in human cytomegalovirus infection. Open Biol. *7*, 160298.

23. Merkulova, M., Păunescu, T.G., Azroyan, A., Marshansky, V., Breton, S., and Brown, D. (2015). Mapping the H(+) (V)-ATPase interactome: identification of proteins involved in trafficking, folding, assembly and phosphorylation. Sci. Rep. *5*, 14827.

24. Carbon, S., Ireland, A., Mungall, C.J., Shu, S., Marshall, B., and Lewis, S.; AmiGO Hub; Web Presence Working Group (2009). AmiGO: online access to ontology and annotation data. Bioinformatics *25*, 288–289.

25. Breyer, F., Härtlova, A., Thurston, T., Flynn, H.R., Chakravarty, P., Janzen, J., Peltier, J., Heunis, T., Snijders, A.P., Trost, M., et al. (2021). TPL-2 kinase induces phagosome acidification to promote macrophage killing of bacteria. EMBO J. *40*, e106188.

26. Kraemer, C., Enklaar, T., Zabel, B., and Schmidt, E.R. (2000). Mapping and structure of DMXL1, a human homologue of the DmX gene from Drosophila melanogaster coding for a WD repeat protein. Genomics *64*, 97–101.

27. Jaskolka, M.C., Winkley, S.R., and Kane, P.M. (2021). RAVE and Rabconnectin-3 Complexes as Signal Dependent Regulators of Organelle Acidification. Front. Cell Dev. Biol. *9*, 698190.

28. Kawabe, H., Sakisaka, T., Yasumi, M., Shingai, T., Izumi, G., Nagano, F., Deguchi-Tawarada, M., Takeuchi, M., Nakanishi, H., and Takai, Y. (2003). A novel rabconnectin-3-binding protein that directly binds a GDP/GTP exchange protein for Rab3A small G protein implicated in Ca(2+)-dependent exocytosis of neurotransmitter. Genes Cells *8*, 537–546.

29. Kane, P.M. (2012). Targeting reversible disassembly as a mechanism of controlling V-ATPase activity. Curr. Protein Pept. Sci. *13*, 117–123.

30. Pavel, M., Imarisio, S., Menzies, F.M., Jimenez-Sanchez, M., Siddiqi, F.H., Wu, X., Renna, M., O'Kane, C.J., Crowther, D.C., and Rubinsztein, D.C. (2016). CCT complex restricts neuropathogenic protein aggregation via autophagy. Nat. Commun. *7*, 13821.

31. Tang, Q., Liu, M., Liu, Y., Hwang, R.D., Zhang, T., and Wang, J. (2021). NDST3 deacetylates alpha-tubulin and suppresses V-ATPase assembly and lysosomal acidification. EMBO J. *40*, e107204.

32. Coffey, E.E., Beckel, J.M., Laties, A.M., and Mitchell, C.H. (2014). Lysosomal alkalization and dysfunction in human fibroblasts with the Alzheimer's disease-linked presenilin 1 A246E mutation can be reversed with cAMP. Neuroscience *263*, 111–124.

33. Brown, B., Siddique, N., and Greene, J. (2022). Herpes Simplex Virus Type 1 and Varicella-Zoster Virus Coinfection in an Immunocompromised Male Patient. Infect. Dis. Clin. Pract. *30*, e1155.

34. Yim, W.W., and Mizushima, N. (2020). Lysosome biology in autophagy. Cell Discov. *6*, 6.

35. Kabeya, Y., Mizushima, N., Ueno, T., Yamamoto, A., Kirisako, T., Noda, T., Kominami, E., Ohsumi, Y., and Yoshimori, T. (2000). LC3, a mammalian homologue of yeast Apg8p, is localized in autophagosome membranes after processing. EMBO J. *19*, 5720–5728.

36. Tanida, I., Ueno, T., and Kominami, E. (2004). LC3 conjugation system in mammalian autophagy. Int. J. Biochem. Cell Biol. *36*, 2503–2518.

37. Klionsky, D.J., Abdalla, F.C., Abeliovich, H., Abraham, R.T., Acevedo-Arozena, A., Adeli, K., Agholme, L., Agnello, M., Agostinis, P., Aguirre-Ghiso, J.A., et al. (2012). Guidelines for the use and interpretation of assays for monitoring autophagy. Autophagy *8*, 445–544.

38. Sarkar, S., Davies, J.E., Huang, Z., Tunnacliffe, A., and Rubinsztein, D.C. (2007). Trehalose, a novel mTOR-independent autophagy enhancer, accelerates the clearance of mutant huntingtin and alpha-synuclein. J. Biol. Chem. *282*, 5641–5652.

39. Klionsky, D.J., Elazar, Z., Seglen, P.O., and Rubinsztein, D.C. (2008). Does bafilomycin A1 block the fusion of autophagosomes with lysosomes? Autophagy *4*, 849–850.

40. Nobre, L.V., Nightingale, K., Ravenhill, B.J., Antrobus, R., Soday, L., Nichols, J., Davies, J.A., Seirafian, S., Wang, E.C., Davison, A.J., et al. (2019). Human cytomegalovirus interactome analysis identifies degradation hubs, domain associations and viral protein functions. eLife *8*, e49894.

41. Boya, P., Reggiori, F., and Codogno, P. (2013). Emerging regulation and functions of autophagy. Nat. Cell Biol. *15*, 713–720.

42. Yadavalli, N., and Ferguson, S.M. (2023). LRRK2 suppresses lysosome degradative activity in macrophages and microglia through MiT-TFE transcription factor inhibition. Proc. Natl. Acad. Sci. USA *120*, e2303789120.

43. Tandon, R., and Mocarski, E.S. (2012). Viral and host control of cytomegalovirus maturation. Trends Microbiol. *20*, 392–401.

44. Close, W.L., Anderson, A.N., and Pellett, P.E. (2018). Betaherpesvirus Virion Assembly and Egress. Adv. Exp. Med. Biol. *1045*, 167–207.

45. Lučin, P., Jug Vučko, N., Karleuša, L., Mahmutefendić Lučin, H., Blagojević Zagorac, G., Lisnić, B., Pavišić, V., Marcelić, M., Grabušić, K., Brizić, I., et al. (2020). Cytomegalovirus Generates Assembly Compartment in the Early Phase of Infection by Perturbation of Host-Cell Factors Recruitment at the Early Endosome/Endosomal Recycling Compartment/Trans-Golgi Interface. Front. Cell Dev. Biol. *8*, 563607.

46. Das, S., Vasanji, A., and Pellett, P.E. (2007). Three-dimensional structure of the human cytomegalovirus cytoplasmic virion assembly complex includes a reoriented secretory apparatus. J. Virol. *81*, 11861–11869.

47. Taisne, C., Lussignol, M., Hernandez, E., Moris, A., Mouna, L., and Esclatine, A. (2019). Human cytomegalovirus hijacks the autophagic machinery and LC3 homologs in order to optimize cytoplasmic envelopment of mature infectious particles. Sci. Rep. *9*, 4560.

48. Stanton, R.J., Baluchova, K., Dargan, D.J., Cunningham, C., Sheehy, O., Seirafian, S., McSharry, B.P., Neale, M.L., Davies, J.A., Tomasec, P., et al. (2010). Reconstruction of the complete human cytomegalovirus genome in a BAC reveals RL13 to be a potent inhibitor of replication. J. Clin. Invest. *120*, 3191–3208.

49. Crump, C. (2018). Virus Assembly and Egress of HSV. Adv. Exp. Med. Biol. *1045*, 23–44.

50. Ma, L., Ouyang, Q., Werthmann, G.C., Thompson, H.M., and Morrow, E.M. (2017). Live-cell Microscopy and Fluorescence-based Measurement of Luminal pH in Intracellular Organelles. Front. Cell Dev. Biol. *5*, 71.

51. Halcrow, P., Khan, N., Datta, G., Ohm, J.E., Chen, X., and Geiger, J.D. (2019). Importance of measuring endolysosome, cytosolic, and extracellular pH in understanding the pathogenesis of and possible treatments for glioblastoma multiforme. Cancer Rep. (Hoboken) *2*, e1193.

52. Pavelin, J., Reynolds, N., Chiweshe, S., Wu, G., Tiribassi, R., and Grey, F. (2013). Systematic microRNA analysis identifies ATP6V0C as an essential host factor for human cytomegalovirus replication. PLoS Pathog. *9*, e1003820.

53. Bénaroch, P., Yilla, M., Raposo, G., Ito, K., Miwa, K., Geuze, H.J., and Ploegh, H.L. (1995). How MHC class II molecules reach the endocytic pathway. EMBO J. *14*, 37–49.

54. Macfarlane, D.E., and Manzel, L. (1998). Antagonism of immunostimulatory CpG-oligodeoxynucleotides by quinacrine, chloroquine, and structurally related compounds. J. Immunol. *160*, 1122–1131.

55. Schwartz, M., Shnayder, M., Nachshon, A., Arazi, T., Kitsberg, Y., Levi Samia, R., Lavi, M., Kuint, R., Tsabari, R., and Stern-Ginossar, N. (2023). Molecular characterization of human cytomegalovirus infection with single-cell transcriptomics. Nat. Microbiol. *8*, 455–468.

56. Dunn, W., Chou, C., Li, H., Hai, R., Patterson, D., Stolc, V., Zhu, H., and Liu, F. (2003). Functional profiling of a human cytomegalovirus genome. Proc. Natl. Acad. Sci. USA *100*, 14223–14228.

57. Wilkinson, G.W., Davison, A.J., Tomasec, P., Fielding, C.A., Aicheler, R., Murrell, I., Seirafian, S., Wang, E.C., Weekes, M., Lehner, P.J., et al. (2015). Human cytomegalovirus: taking the strain. Med. Microbiol. Immunol. *204*, 273–284.

58. Gatherer, D., Seirafian, S., Cunningham, C., Holton, M., Dargan, D.J., Baluchova, K., Hector, R.D., Galbraith, J., Herzyk, P., Wilkinson, G.W., et al. (2011). High-resolution human cytomegalovirus transcriptome. Proc. Natl. Acad. Sci. USA *108*, 19755–19760.

59. Jean Beltran, P.M., Mathias, R.A., and Cristea, I.M. (2016). A portrait of the human organelle proteome in space and time during Cytomegalovirus infection. Cell Syst. *3*, 361–373.e6.

60. Lussignol, M., and Esclatine, A. (2017). Herpesvirus and Autophagy: "All Right, Everybody Be Cool, This Is a Robbery!". Viruses *9*, 372.

61. Chaumorcel, M., Lussignol, M., Mouna, L., Cavignac, Y., Fahie, K., Cotte-Laffitte, J., Geballe, A., Brune, W., Beau, I., Codogno, P., et al. (2012). The human cytomegalovirus protein TRS1 inhibits autophagy via its interaction with Beclin 1. J. Virol. *86*, 2571–2584.

62. McFarlane, S., Aitken, J., Sutherland, J.S., Nicholl, M.J., Preston, V.G., and Preston, C.M. (2011). Early Induction of Autophagy in Human Fibroblasts after Infection with Human Cytomegalovirus or Herpes Simplex Virus 1. J. Virol. *85*, 4212–4221.

63. Mouna, L., Hernandez, E., Bonte, D., Brost, R., Amazit, L., Delgui, L.R., Brune, W., Geballe, A.P., Beau, I., and Esclatine, A. (2016). Analysis of the role of autophagy inhibition by two complementary human cytomegalovirus BECN1/Beclin 1-binding proteins. Autophagy *12*, 327–342.

64. Ishida, T., and Ciulli, A. (2021). E3 Ligase Ligands for PROTACs: How They Were Found and How to Discover New Ones. SLAS Discov. *26*, 484–502.

65. McGeoch, D.J., Rixon, F.J., and Davison, A.J. (2006). Topics in herpesvirus genomics and evolution. Virus Res. *117*, 90–104.

66. Cagliani, R., Forni, D., Mozzi, A., and Sironi, M. (2020). Evolution and Genetic Diversity of Primate Cytomegaloviruses. Microorganisms *8*, 624.

67. Altschul, S.F., Gish, W., Miller, W., Myers, E.W., and Lipman, D.J. (1990). Basic local alignment search tool. J. Mol. Biol. *215*, 403–410.

68. Murthy, S., O'Brien, K., Agbor, A., Angedakin, S., Arandjelovic, M., Ayimisin, E.A., Bailey, E., Bergl, R.A., Brazzola, G., Dieguez, P., et al. (2019). Cytomegalovirus distribution and evolution in hominines. Virus Evol. *5*, vez015.

69. Perreira, J.M., Aker, A.M., Savidis, G., Chin, C.R., McDougall, W.M., Portmann, J.M., Meraner, P., Smith, M.C., Rahman, M., Baker, R.E., et al. (2015). RNASEK Is a V-ATPase-Associated Factor Required for Endocytosis and the Replication of Rhinovirus, Influenza A Virus, and Dengue Virus. Cell Rep. *12*, 850–863.

70. Guinea, R., and Carrasco, L. (1995). Requirement for vacuolar proton-ATPase activity during entry of influenza virus into cells. J. Virol. *69*, 2306–2312.

71. Ochiai, H., Sakai, S., Hirabayashi, T., Shimizu, Y., and Terasawa, K. (1995). Inhibitory effect of bafilomycin A1, a specific inhibitor of vacuolar-type proton pump, on the growth of influenza A and B viruses in MDCK cells. Antiviral Res. *27*, 425–430.

72. Icho, S., Rujas, E., Muthuraman, K., Tam, J., Liang, H., Landreth, S., Liao, M., Falzarano, D., Julien, J.P., and Melnyk, R.A. (2022). Dual Inhibition of Vacuolar-ATPase and TMPRSS2 Is Required for Complete Blockade of SARS-CoV-2 Entry into Cells. Antimicrob. Agents Chemother. *66*, e0043922.

73. Schuchman, R.M., Vancini, R., Piper, A., Breuer, D., Ribeiro, M., Ferreira, D., Magliocca, J., Emmerich, V., Hernandez, R., and Brown, D.T. (2018). Role of the vacuolar ATPase in the Alphavirus replication cycle. Heliyon *4*, e00701.

74. Yan, Y., Jiang, K., Liu, P., Zhang, X., Dong, X., Gao, J., Liu, Q., Barr, M.P., Zhang, Q., Hou, X., et al. (2016). Bafilomycin A1 induces caspase-independent cell death in hepatocellular carcinoma cells via targeting of autophagy and MAPK pathways. Sci. Rep. *6*, 37052.

75. Vanarsdall, A.L., Wisner, T.W., Lei, H., Kazlauskas, A., and Johnson, D.C. (2012). PDGF receptor-alpha does not promote HCMV entry into epithelial and endothelial cells but increased quantities stimulate entry by an abnormal pathway. PLoS Pathog. *8*, e1002905.

76. Ryckman, B.J., Jarvis, M.A., Drummond, D.D., Nelson, J.A., and Johnson, D.C. (2006). Human cytomegalovirus entry into epithelial and endothelial cells depends on genes UL128 to UL150 and occurs by endocytosis and low-pH fusion. J. Virol. *80*, 710–722.

77. Wang, D., Yu, Q.C., Schröer, J., Murphy, E., and Shenk, T. (2007). Human cytomegalovirus uses two distinct pathways to enter retinal pigmented epithelial cells. Proc. Natl. Acad. Sci. USA *104*, 20037–20042.

78. Vanarsdall, A.L., and Johnson, D.C. (2012). Human cytomegalovirus entry into cells. Curr. Opin. Virol. *2*, 37–42.

79. He, Y., Xu, Y., Zhang, C., Gao, X., Dykema, K.J., Martin, K.R., Ke, J., Hudson, E.A., Khoo, S.K., Resau, J.H., et al. (2011). Identification of a lysosomal pathway that modulates glucocorticoid signaling and the inflammatory response. Sci. Signal. *4*, ra44.

80. Fois, G., Hobi, N., Felder, E., Ziegler, A., Miklavc, P., Walther, P., Radermacher, P., Haller, T., and Dietl, P. (2015). A new role for an old drug: Ambroxol triggers lysosomal exocytosis via pH-dependent Ca^{2+} release from acidic Ca^{2+} stores. Cell Calcium *58*, 628–637.

81. Ziegler, H.K., and Unanue, E.R. (1982). Decrease in macrophage antigen catabolism caused by ammonia and chloroquine is associated with inhibition of antigen presentation to T cells. Proc. Natl. Acad. Sci. USA *79*, 175–178.

82. Xiu, Y., Xu, H., Zhao, C., Li, J., Morita, Y., Yao, Z., Xing, L., and Boyce, B.F. (2014). Chloroquine reduces osteoclastogenesis in murine osteoporosis by preventing TRAF3 degradation. J. Clin. Invest. *124*, 297–310.

83. Vomero, M., Barbati, C., Colasanti, T., Perricone, C., Novelli, L., Ceccarelli, F., Spinelli, F.R., Di Franco, M., Conti, F., Valesini, G., et al. (2018). Autophagy and Rheumatoid Arthritis: Current Knowledges and Future Perspectives. Front. Immunol. *9*, 1577.

84. Kuznik, A., Bencina, M., Svajger, U., Jeras, M., Rozman, B., and Jerala, R. (2011). Mechanism of endosomal TLR inhibition by antimalarial drugs and imidazoquinolines. J. Immunol. *186*, 4794–4804.

85. Redmann, M., Benavides, G.A., Berryhill, T.F., Wani, W.Y., Ouyang, X., Johnson, M.S., Ravi, S., Barnes, S., Darley-Usmar, V.M., and Zhang, J. (2017). Inhibition of autophagy with bafilomycin and chloroquine decreases mitochondrial quality and bioenergetic function in primary neurons. Redox Biol. *11*, 73–81.

86. Kondo, H., Maksimova, N., Otomo, T., Kato, H., Imai, A., Asano, Y., Kobayashi, K., Nojima, S., Nakaya, A., Hamada, Y., et al. (2017). Mutation in VPS33A affects metabolism of glycosaminoglycans: a new

type of mucopolysaccharidosis with severe systemic symptoms. Hum. Mol. Genet. *26*, 173–183.

87. Soyombo, A.A., Tjon-Kon-Sang, S., Rbaibi, Y., Bashllari, E., Bisceglia, J., Muallem, S., and Kiselyov, K. (2006). TRP-ML1 regulates lysosomal pH and acidic lysosomal lipid hydrolytic activity. J. Biol. Chem. *281*, 7294–7301.
88. Kogot-Levin, A., Zeigler, M., Ornoy, A., and Bach, G. (2009). Mucolipidosis type IV: the effect of increased lysosomal pH on the abnormal lysosomal storage. Pediatr. Res. *65*, 686–690.
89. Stanton, R.J., McSharry, B.P., Armstrong, M., Tomasec, P., and Wilkinson, G.W. (2008). Re-engineering adenovirus vector systems to enable high-throughput analyses of gene function. BioTechniques *45*, 659–668.
90. Stanton, R.J., McSharry, B.P., Rickards, C.R., Wang, E.C., Tomasec, P., and Wilkinson, G.W. (2007). Cytomegalovirus destruction of focal adhesions revealed in a high-throughput Western blot analysis of cellular protein expression. J. Virol. *81*, 7860–7872.
91. Barger, C.J., Branick, C., Chee, L., and Karpf, A.R. (2019). Pan-Cancer Analyses Reveal Genomic Features of FOXM1 Overexpression in Cancer. Cancers (Basel) *11*, 251.
92. Puri, C., Vicinanza, M., Ashkenazi, A., Gratian, M.J., Zhang, Q., Bento, C.F., Renna, M., Menzies, F.M., and Rubinsztein, D.C. (2018). The RAB11A-Positive Compartment Is a Primary Platform for Autophagosome Assembly Mediated by WIPI2 Recognition of PI3P-RAB11A. Dev. Cell *45*, 114–131.e8.
93. da Huang, W., Sherman, B.T., and Lempicki, R.A. (2009). Systematic and integrative analysis of large gene lists using DAVID bioinformatics resources. Nat. Protoc. *4*, 44–57.
94. Vizcaíno, J.A., Csordas, A., del-Toro, N., Dianes, J.A., Griss, J., Lavidas, I., Mayer, G., Perez-Riverol, Y., Reisinger, F., Ternent, T., et al. (2016). 2016 update of the PRIDE database and its related tools. Nucleic Acids Res. *44*, D447–D456.
95. Menzies, S.A., Volkmar, N., van den Boomen, D.J., Timms, R.T., Dickson, A.S., Nathan, J.A., and Lehner, P.J. (2018). The sterol-responsive RNF145 E3 ubiquitin ligase mediates the degradation of HMG-CoA reductase together with gp78 and Hrd1. eLife *7*, e40009.
96. Dolan, A., Cunningham, C., Hector, R.D., Hassan-Walker, A.F., Lee, L., Addison, C., Dargan, D.J., McGeoch, D.J., Gatherer, D., Emery, V.C., et al. (2004). Genetic content of wild-type human cytomegalovirus. J. Gen. Virol. *85*, 1301–1312.
97. McSharry, B.P., Jones, C.J., Skinner, J.W., Kipling, D., and Wilkinson, G.W.G. (2001). Human telomerase reverse transcriptase-immortalized MRC-5 and HCA2 human fibroblasts are fully permissive for human cytomegalovirus. J. Gen. Virol. *82*, 855–863.
98. Gierasch, W.W., Zimmerman, D.L., Ward, S.L., Vanheyningen, T.K., Romine, J.D., and Leib, D.A. (2006). Construction and characterization of bacterial artificial chromosomes containing HSV-1 strains 17 and KOS. J. Virol. Methods *135*, 197–206.
99. Tischer, B.K., Smith, G.A., and Osterrieder, N. (2010). En passant mutagenesis: a two step markerless red recombination system. Methods Mol. Biol. *634*, 421–430.
100. McAlister, G.C., Nusinow, D.P., Jedrychowski, M.P., Wühr, M., Huttlin, E.L., Erickson, B.K., Rad, R., Haas, W., and Gygi, S.P. (2014). MultiNotch MS3 enables accurate, sensitive, and multiplexed detection of differential expression across cancer cell line proteomes. Anal. Chem. *86*, 7150–7158.
101. McAlister, G.C., Huttlin, E.L., Haas, W., Ting, L., Jedrychowski, M.P., Rogers, J.C., Kuhn, K., Pike, I., Grothe, R.A., Blethrow, J.D., et al. (2012). Increasing the multiplexing capacity of TMTs using reporter ion isotopologues with isobaric masses. Anal. Chem. *84*, 7469–7478.
102. Albarnaz, J.D., Ren, H., Torres, A.A., Shmeleva, E.V., Melo, C.A., Bannister, A.J., Brember, M.P., Chung, B.Y., and Smith, G.L. (2022). Molecular mimicry of NF-κB by vaccinia virus protein enables selective inhibition of antiviral responses. Nat. Microbiol. *7*, 154–168.
103. Stern-Ginossar, N., Weisburd, B., Michalski, A., Le, V.T., Hein, M.Y., Huang, S.X., Ma, M., Shen, B., Qian, S.B., Hengel, H., et al. (2012). Decoding human cytomegalovirus. Science *338*, 1088–1093.
104. Huttlin, E.L., Jedrychowski, M.P., Elias, J.E., Goswami, T., Rad, R., Beausoleil, S.A., Villén, J., Haas, W., Sowa, M.E., and Gygi, S.P. (2010). A tissue-specific atlas of mouse protein phosphorylation and expression. Cell *143*, 1174–1189.
105. Cox, J., and Mann, M. (2008). MaxQuant enables high peptide identification rates, individualized p.p.b.-range mass accuracies and proteome-wide protein quantification. Nat. Biotechnol. *26*, 1367–1372.
106. Costes, S.V., Daelemans, D., Cho, E.H., Dobbin, Z., Pavlakis, G., and Lockett, S. (2004). Automatic and quantitative measurement of protein-protein colocalization in live cells. Biophys. J. *86*, 3993–4003.
107. Tunyasuvunakool, K., Adler, J., Wu, Z., Green, T., Zielinski, M., Žídek, A., Bridgland, A., Cowie, A., Meyer, C., Laydon, A., et al. (2021). Highly accurate protein structure prediction for the human proteome. Nature *596*, 590–596.
108. Jahreiss, L., Menzies, F.M., and Rubinsztein, D.C. (2008). The itinerary of autophagosomes: from peripheral formation to kiss-and-run fusion with lysosomes. Traffic *9*, 574–587.

STAR★METHODS

KEY RESOURCES TABLE

REAGENT or RESOURCE	SOURCE	IDENTIFIER
Antibodies		
Rabbit polyclonal anti-LC3B	Abcam	Cat#ab48394, RRID: AB_881433
Mouse monoclonal anti-RNF123	Santa Cruz Biotechnology	Cat# sc-101122, RRID: AB_2182272
Mouse monoclonal anti-UBAC1	Proteintech	Cat# 67385-1-Ig, RRID: AB_2882630
Rabbit polyclonal anti-DMXL1	Bethyl	Cat# A304-685A, RRID: AB_2620880
Mouse monoclonal anti-HCMV IE1/2	Merk	Cat# MAB810R, RRID: AB_570324
Mouse monoclonal anti-GAPDH	R&D Systems	Cat#MAB5718, RRID: AB_10892505
Rabbit polyclonal anti-Calnexin	LSBio	Cat# LS-B6881-100, RRID: AB_11186721
Rabbit monoclonal anti-V5	Cell Signaling Technology	Cat# 13202, RRID: AB_2687461
Mouse monoclonal anti-CD107a (LAMP1)	BioLegend	Cat# 328602, RRID: AB_1134259
Rabbit polyclonal anti-Giantin	Abcam	Cat# ab80864, RRID: AB_10670397
Mouse monoclonal anti-HCMV gB	Abcam	Cat# ab6499, RRID: AB_305519
Goat polyclonal anti-Adenovirus	Chemicon	Cat# AB1056 RRID: AB_11212049
IRDye 680RD goat anti-mouse IgG	LI-COR	Cat#925-68070, RRID: AB_2651128
IRDye 800CW goat anti-rabbit IgG	LI-COR	Cat#925-32211, RRID: AB_2651127
Goat anti-rabbit IgG Alexa Flour 568	Thermo Fisher Scientific	Cat# A-11011, RRID: AB_143157
Goat anti-mouse IgG Alexa Flour 647	Thermo Fisher Scientific	Cat# A-21235, RRID: AB_2535804
Mouse anti-goat IgG-HRP	Santa Cruz Biotechnology	Cat# sc-2354, RRID: AB_628490
Horse anti-mouse IgG-HRP	Cell Signaling Technology	Cat #7076, RRID: AB_330924
Goat anti-rabbit IgG-HRP	Cell Signaling Technology	Cat #7074, RRID: AB_2099233
Human TruStain FcX	BioLegend	Cat#422302
Bacterial and virus strains		
HCMV Merlin	Stanton et al.[48]	RCMV1111
HCMV Merlin UL36-GFP	This paper	RCMV2582
HCMV AD169-GFP	Fielding et al.[15]	RCMV288
HCMV Merlin ΔUS29	This paper	RCMV3082
HCMV Merlin ΔUS30	This paper	RCMV3066
HCMV Merlin ΔUS31	This paper	RCMV3083
HCMV Merlin ΔUS32	This paper	RCMV3045
HCMV Merlin ΔUS33A	This paper	RCMV3037
HCMV Merlin ΔUS34	This paper	RCMV2936
HCMV Merlin ΔUS34A	This paper	RCMV2935
HSV-1 UL47-EYFP	This paper	N/A
E. coli. (α-Select Silver Competent Cells)	Bioline	Cat#BIO-85026
Adenovirus expressing US33A	Stanton et al.[89]	N/A
Chemicals, peptides, and recombinant proteins		
Tandem mass tag (TMT) 10-plex isobaric reagents	Thermo Fisher	Cat#90110
HPLC water	VWR	Cat#23595.328
LC-MS grade Acetonitrile	Merck	Cat#1.00029.2500
Formic acid	Thermo Fisher	Cat#85178
DL-Dithiothreitol (DTT)	Sigma	Cat#43815-1G
Acetonitrile, Extra Dry	Extra Dry Acros Organics	Cat#AC364311000

(*Continued on next page*)

Continued

REAGENT or RESOURCE	SOURCE	IDENTIFIER
Hydroxylamine	Sigma	Cat#438227
DPBS	Sigma	Cat#D8537-500ML
DMEM	Sigma	Cat#D6429-500ML
Phenol-red free DMEM	Gibco	Cat#31053028
FBS	Sigma	Cat#F7524-500ML Lot#0001640350
Puromycin	InvivoGen	Cat# ant-pr-1
Trypsin-EDTA	Gibco	Cat# 25300-054
Bovine serum albumin	Sigma-Aldrich	Cat# A7906
HEPES (1M, pH7.0-7.6)	Sigma-Aldrich	Cat# H0887
Guanidine hydrochloride (8M)	Thermo Fisher Scientific	Cat# 24115
Bafilomycin A	Enzo	Cat# BML-CM110-0100
Complete Protease Inhibitor Cocktail	Roche	Cat# 11836153001
Fixation Buffer	BioLegend	Cat# 420801
DMSO	Sigma-Aldrich	Cat# D8418
Dexamethasone	Sigma-Aldrich	Cat# D4902
DAPI	Cell Signaling	Cat# 4083S
Nonidet P-40 (NP-40)	Sigma-Aldrich	Cat# 75385-1L
Glycerol	Sigma-Aldrich	Cat# G7757-1L
Triton X-100	Sigma	Cat# X100-500ML
4% fixation buffer	BioLegend	Cat# 420081
Sodium dodecyl sulfate	Fisher Chemical	Cat# S/P530/53
Critical commercial assays		
BCA Protein Assay Kit	Thermo Fisher	Cat#23227
Micro BCA Protein Assay Kit	Thermo Fisher	Cat#23235
RNeasy Plus Kit	Qiagen	Cat#74134
RNeasy Mini Kit	Qiagen	Cat#74104
QIAprep Spin Miniprep Kit	Qiagen	Cat#27104
QIAquick Gel Extraction Kit	Qiagen	Cat#28704
GoScript Reverse Transcriptase kit	Promega	Cat#A5001
TaqMan™ Universal PCR Master Mix	Thermo Fisher	Cat#4304437
LysoTracker Red DND-99	Invitrogen	Cat#L7528
LysoSensor Yellow/Blue DND-160	Invitrogen	Cat#L7545
HCS CellMask Blue Stain	Invitrogen	Cat#H32730
Lipofectamine 3000 transfection reagent	Invitrogen	Cat#L3000001
TaqMan Universal PCR Master Mix	Invitrogen	Cat#4304437
Fast SYBR Green PCR Master Mix	Invitrogen	Cat#4385612
NEBuilder HiFi DNA Assembly Master Mix	NEB	Cat#E2621S
P3 primary cell 4D-Nucleofector X kit	Lonza	Cat#V4XP-3032
MluI-HF restriction enzyme rCutSmart	NEB	Cat#R3198S
NheI-HF restriction enzyme rCutSmart	NEB	Cat#R3131S
SuperSignal West Pico Chemiluminescent Substrate	Thermo Scientific	Cat#34080
Deposited data		
Raw Mass Spectrometry Data Files	This paper	ProteomeXchange Consortium via the PRIDE partner repository, with the dataset identifier PXD044273.

(*Continued on next page*)

Continued

REAGENT or RESOURCE	SOURCE	IDENTIFIER
Unprocessed peptide file for Figure 1	This paper	https://data.mendeley.com/datasets/rvjz3wbz9m/draft?a=318040f4-52fd-49b5-bd21-cdb0a3343173
Experimental models: Cell lines		
HFFF immortalized with human telomerase (HFFF-TERT)	Stanton et al.[90]	N/A
HFFF expressing the coxsackie virus and adenovirus receptor (HFFF-CAR)	Stanton et al.[89]	N/A
HEK293T	ATCC	N/A
ARPE-19	ATCC	N/A
Oligonucleotides		
Forward primer for cloning US33A into Adenovirus vectors: AACCGTCAGATC GCCTGGAGACGCCATCCACGCTGTT TTGACCTCCATAGAAGACACCGGGA CCGATCCAGCCTGGATCCACCATGA GCCTCAGGTTCCC	This paper	N/A
Reverse primer for cloning US33A into Adenovirus vectors: CACAGGCGTGA CACGTTTATTGAGTAGGATTACAGAG TATAACATAGAGTATAATATAGAGTAT ACAATAGTGACGTGGGATCCCTAGG ACCGCGGCACG	This paper	N/A
Oligonucleotide 1 for pHAGE-pSFFV-Control construct: GGGGACAAGTTTGTA CAAAAAAGCAGGCTCCCAGGCGAGAA CGTGTGCGTGGACAAGCGAGCAGCAT ACGAACCCAGCTTTCTTGTACAAAGTG GTCCCC	Nightingale et al.[7]	N/A
Oligonucleotide 2 for pHAGE-pSFFV-Control construct: GGGGACCACTTTGTA CAAGAAAGCTGGGTTCGTATGCTGCT CGCTTGTCCACGCACACGTTCTCGCC TGGGAGCCTGCTTTTTTGTACAAACTT GTCCCC	Nightingale et al.[7]	N/A
Forward primer for pHAGE-pSFFV-US33A construct: GGGGACAAGTT TGTACAAAAAAGCAGGCTATGAG CCTCAGGTTCCCCG	This paper	N/A
Reverse primer for pHAGE-pSFFV-US33A construct: GGGGACCA CTTTGTACAAGAAAGCTGGGTTT AGGACCGCGGCACGTAAAAC	This paper	N/A
Forward primer for pHAGE-pSFFV-V5-SA-US33A construct: GGGGACAAGTTTGT ACAAAAAAGCAGGCTATGGGTAAGCCA ATCCCTAACCCGCTCCTAGGTCTTGA TTCTACGAGCGCTAGCCTCAGGTTCC CCGAG	This paper	N/A
Reverse primer for pHAGE-pSFFV-V5-SA-US33A construct: GGGGACCACTTTGTAC AAGAAAGCTGGGTTTAGGACCGCGGCA CGTAAAAC	This paper	N/A

(*Continued on next page*)

Continued

REAGENT or RESOURCE	SOURCE	IDENTIFIER
Forward primer for pHAGE-pSFFV-V5-GGGS-US33A construct: GGGGACAAGTTTGTACAAAAAAGCAGGCTATGGGTAAGCCAATCCCTAACCCGCTCCTAGGTCTTGATTCTACGGGAGGTGGATCAAGCCTCAGGTTCCCCGAG	This paper	N/A
Reverse primer for pHAGE-pSFFV-V5-GGGS-US33A construct: GGGGACCACTTTGTACAAGAAAGCTGGGTTTAGGACCGCGGCACGTAAAAC	This paper	N/A
Forward primer for pHAGE-pSFFV-US33A-GGGS-V5 construct: GGGGACAAGTTTGTACAAAAAAGCAGGCTATGAGCCTCAGGTTCCCCG	This paper	N/A
Reverse primer for pHAGE-pSFFV-US33A-GGGS-V5 construct: GGGGACCACTTTGTACAAGAAAGCTGGGTTTACGTAGAATCAAGACCTAGGAGCGGGTTAGGGATTGGCTTACCTGATCCACCTCCGGACCGCGGCACGTAAAAC	This paper	N/A
Forward primer for HCMV US33A RT-qPCR: GGGTTACGAGAAACTGGGATAC	This paper	N/A
Reverse primer for HCMV US33A RT-qPCR: AACGGAAAAGTGAACGGCAA	This paper	N/A
Forward primer for GAPDH RT-qPCR: CCAGTAAGTGCGGGTAATAAGC	This paper	N/A
Reverse primer for GAPDH RT-qPCR: GAGCCCCAGCCTTCTCCATG	This paper	N/A
Forward primer for 18S RT-qPCR: CCAGTAAGTGCGGGTAATAAGC	This paper	N/A
Reverse primer for 18S RT-qPCR: GCCTCACTAAACCATCCAATCGG	This paper	N/A
Forward primer for US33A-V5 RT-qPCR: GGGTTACGAGAAACTGGGATAC	This paper	N/A
Reverse primer for US33A-V5 RT-qPCR: GCGGGTTAGGGATTGGCTTAC	This paper	N/A
Forward primer for US33A-V5-C RT-qPCR: GCTGGTGTTGCCGTTCACT	This paper	N/A
Reverse primer for US33A-V5-C RT-qPCR: CGTAGAATCAAGACCTAGGAGCG	This paper	N/A
Forward primer for US33A-V5-N RT-qPCR: AGAGGGCGGGTTACGAGAA	This paper	N/A
Reverse primer for US33A-V5-N RT-qPCR: GCGGGTTAGGGATTGGCTTA	This paper	N/A
Forward primer for US33A-V5-αH RT-qPCR: GCATGACCCGTTGGGATTGA	This paper	N/A
Reverse primer for US33A-V5-αH RT-qPCR: CGTAGAATCAAGACCTAGGAGCG	This paper	N/A
COL444: CGCACGTGTCGGGGAGGCGCGCGACCGGGCTGGGAGGCCCGCCACGCCCAGTGAGCAAGGGCGAGGAG	This paper	N/A
COL445: GTTATGCCGCGTCCAGGGCCATCGGGGCGCTTTTTATCGGGAGGAGCTTACTTGTACAGCTCGTCCATG	This paper	N/A
Please refer to Table S5 for complete oligonucleotides including those for shRNA and CRISPR/Cas9 gene disruption		

(*Continued on next page*)

Continued

REAGENT or RESOURCE	SOURCE	IDENTIFIER
Recombinant DNA		
pHAGE-pSFFV	This paper	N/A
pHAGE-pSFFV-Control	This paper	N/A
pHAGE-pSFFV-US33A	This paper	N/A
pHAGE-pSFFV-V5-SA-US33A	This paper	N/A
pHAGE-pSFFV-V5-GGGS-US33A	This paper	N/A
pHAGE-pSFFV-US33A-GGGS-V5	This paper	N/A
pHAGE-pSFFV-US33A-SA-V5	Nobre et al.[8]	N/A
pCW57.1-US33A-V5	This paper	N/A
pCW57.1-US33A-V5_ΔN	This paper	N/A
pCW57.1-US33A-V5_ΔαH	This paper	N/A
pCW57.1-US33A-V5_ΔC	This paper	N/A
pCW57.1-US33A-V5_ΔN+αH	This paper	N/A
pCW57.1-US33A-V5_ΔαH+C	This paper	N/A
pCW57.1-US33A-V5_ΔN+C	This paper	N/A
pCW57-MCS1-2A-MCS2	Barger et al.[91]	Addgene #71782
mCherry-LC3B	Puri et al.[92]	N/A
CD63-pEGFP	Luzio Lab	Addgene #62964
Software and algorithms		
"MassPike", a Sequest-based software pipeline for quantitative proteomics.	Professor Steven Gygi's lab, Harvard Medical School, Boston, USA.	N/A
DAVID software	Huang da et al.[93]	https://david.ncifcrf.gov/
Image Studio Lite	LI-COR	Ver. 5.2 https://www.licor.com/bio/image-studio/
Image Lab Software	Bio-Rad	https://www.bio-rad.com/en-uk/product/image-lab-software?ID=KRE6P5E8Z
GraphPad Prism 10	GraphPad Software Inc.	https://www.graphpad.com/
BioRender	BioRender.com	https://biorender.com/
FlowJo	Tree Star Inc	Ver. 9 https://www.flowjo.com/solutions/flowjo
ImageJ	NIH	https://imagej.nih.gov/ij/index.html
Volocity	Quorum Technologies Inc.	https://www.volocity4d.com/
ZEN confocal software	Zeiss	https://www.zeiss.com/microscopy/en/products/software/zeiss-zen-lite.html
Other		
Orbitrap Fusion Lumos Mass Spectrometer	ThermoFisher Scientific	Cat# IQLAAEGAAP FADBMBHQ
Fortessa flow cytometer	Becton Dickinson	N/A
Confocal microscopy	Zeiss	LSM880
Amaxa™ 4D-Nucleofector	Lonza	4D-Nucleofector X unit
Bio-Rad 96-well qPCR machine	Bio-Rad	CFX96

RESOURCE AVAILABILITY

Lead contact

Further information and requests for resources and reagents should be directed to and will be fulfilled by the lead contact, Michael P. Weekes (mpw1001@cam.ac.uk).

Materials availability

Materials generated in this study are available on request to the corresponding author.

Data and code availability

Unprocessed peptide data files for Figure 1 are available at https://data.mendeley.com/datasets/rvjz3wbz9m/draft?a=318040f4-52fd-49b5-bd21-cdb0a3343173. This file includes details of peptide sequence, redundancy, protein assignment raw unprocessed TMT reporter intensities, and isolation specificity. The mass spectrometry proteomics data have been deposited to the ProteomeXchange Consortium via the PRIDE[94] partner repository with the dataset identifier PXD044273. No new code was generated in this study. All raw data and any information required to reanalyze the data in this manuscript are available on request.

EXPERIMENTAL MODEL AND SUBJECT DETAILS

Cells and cell culture

Human fetal foreskin fibroblast cells immortalized with human telomerase (HFFF-TERTs, male), HEK293T cells (female), and ARPE-19 cells were grown in Dulbecco's modified Eagle's medium (DMEM) supplemented with fetal bovine serum (FBS: 10% v/v, SIGMA) at 37°C in 5% v/v CO_2. HFFF-TERTs have been tested at regular intervals since isolation to confirm that human leukocyte antigen (HLA) and MHC Class I Polypeptide-Related Sequence A (MICA) genotypes, cell morphology and antibiotic resistance are unchanged. In addition, HCMV strain Merlin grows only in human fibroblast cells (dermal or foreskin in origin), further reducing the possibility that they have been contaminated with another cell type. HEK293T cells were obtained as a gift from Professor Paul Lehner and had been authenticated by Short Tandem Repeat profiling.[95] All cells were confirmed to be mycoplasma-negative (Lonza MycoAlert).

Viruses

The genome sequence of HCMV strain Merlin (GenBAnk accession AY446894) is designated the reference HCMV sequence (RefSeq accession NC_006273.2) by the National Center for Biotechnology Information, and was originally sequenced after three passages in human fibroblast cells.[48,96] A recombinant version (RCMV1111) of this strain was derived by transfection of a sequenced BAC clone.[48] RCMV1111 contains point mutations in two genes (RL13 and UL128) that enhance replication in fibroblasts.[48] HCMV expressing rGFP from a P2A self-cleaving peptide at the 3'-end of the UL36 coding region (RCMV2582) was generated by recombineering the strain Merlin BAC as described previously.[48] The single gene deletion mutants: ΔUS29 (RCMV3082), ΔUS30 (RCMV3066), ΔUS31 (RCMV3083), ΔUS32 (RCMV3045), ΔUS33A (RCMV3037), ΔUS34 (RCMV2936), ΔUS34A (RCMV2935) were generated on a background of RCMV2582 (Table S6). RCMV288 was used for plaque assays, and is based on HCMV strain AD169 with one copy of the EGFP (enhanced green fluorescent protein) gene inserted in one copy of the HCMV long repeat under the control of the HCMV RNA2.7 early promoter.[97] Viral stocks were prepared in HFFF-TERTs as described previously.[90] Viruses were titrated by plating $1.5x10^5$ cells in 12-well plates. After 24 h, cells were infected with viral stocks diluted at 1:16, 1:64, 1:256, 1:1024 in DMEM for 2 h prior to replacement with DMEM+10% FBS. Cells were harvested for flow cytometry at 24 h infection, and the viral titer estimated from the percentage of GFP positive cells. Whole-genome consensus sequences of passage 1 of all recombinant viruses were determined using the Illumina platform as described previously.

A replication deficient recombinant adenovirus vector (RAd) type 5 expressing US33A was made as described previously.[89] In brief, the entire US33A ORF was amplified from HCMV strain Merlin DNA using primers recognizing the 3' or 5' end of US33A (Table S7A) and inserted into pAdZ5 by recombineering. After verifying the insert by Sanger sequencing, vector DNA was purified using Qiagen Plasmid Maxi kit and transfected into 293TREx cells. Virus was amplified in 293TREx cells, extracted using tetrachloroethylene, and titrated by plaque assay on HEK293T monolayers.

A fluorescent HSV-1 strain encoding UL47 with an in-frame C-terminal fusion to EYFP (A206K) was constructed using bacterial artificial chromosome (BAC)-cloned KOS strain of HSV-1[98] and the two-step Red recombination technique[99] using the primers COL444 and COL445 (key resources table). Viral stocks were prepared in Vero cells and titrated using a plaque assay on HFFF-TERT monolayers.

METHOD DETAILS

Viral infections

For HCMV and HSV-1 infection, the required volume of viral stock to achieve the multiplicity of infection (MOI) described in the results section was diluted in the serum-free DMEM, mixed gently and applied to HFFF-TERTs. Mock infections were performed identically but with DMEM instead of viral stock. Time zero was considered the time at which cells first came into contact with virus. Cells were incubated with virus for 2 h at 37C on a rocking platform, and the medium was replaced with DMEM+FBS or DMEM+FBS supplemented with 10 nM BafA1 or DMSO.

For RAd infections, the required volume of viral stock to achieve MOI 5 was diluted in serum-free DMEM, mixed gently, and applied to HFFF-CARs. Expression of the CAR receptor boosts the efficiency of adenovirus infection.[89] Cells were incubated with virus for 2 h at 37C on a rocking platform, then medium was replaced with DMEM+FBS. Cells were infected with RAd for 72 h at 37C before further analysis.

Plasmid construction

US33A was amplified from an adenoviral template, expressing the gene under the control of the HCMV major immediate early promoter (MIEP). Primers were designed to recognize the 3' end of the MIEP (forward) and the 3' end of the gene if untagged (reverse). Both primers had flanking Gateway attB sequences for the purpose of cloning, and where required V5 and additional linker sequences (key resources table; Tables S7B and S7C).[40] PCR employed PfuUltra II Fusion HS DNA polymerase (Agilent). Constructs were subsequently cloned into lentiviral destination vector pHAGE-pSFFV using Gateway system (Thermo Scientific).[7] The untagged version of US33A, US33A with an N-terminal V5 tag separated by a serine-alanine linker (V5-SA-US33A), US33A with an N-terminal V5 tag separated by a glycine-glycine-glycine-serine linker (V5-GGGS-US33A) and US33A with a C-terminal V5 tag separated by a glycine-glycine-glycine-serine linker (US33A-GGGS-V5) were cloned from the pHAGE-pSFFV- US33A-V5 vector (key resources table; Table S7C).

Truncations of US33A-V5 were synthesized as double-stranded DNA fragments (gBlocks, Integrated DNA Technologies, detailed in key resources table, Table S7B). Gene fragments were cloned into a linearized (MluI-HF and NheI-HF (NEB, R3198S, R3131S)), gel-purified doxycycline-inducible lentiviral vector pCW57-MCS1-2A-MCS2 (plasmid #71782, Addgene)[91] via a Gibson Assembly reaction (NEB, E2621S) at a 5:1 ratio.

To generate shRNA constructs, two partially complementary oligonucleotides were annealed, with all sequences shown in Table S7D. The resulting product was ligated as a BamHI-EcoRI fragment into the pHR-SIREN vector (a gift from Prof. Paul Lehner, University of Cambridge) using T4 ligase (Thermo Scientific). All constructed plasmids were transformed into 5-alpha Competent E. coli (NEB) and selected on antibiotic-containing luria broth (LB) agar plates. All plasmid inserts were sequenced fully to check for mutations. Two different non-targeting control shRNA sequences are shown in Table S7D, which also lists the sequences of all primers and oligonucleotides.

Transient transfection of HEK293T cells with US33A truncation mutants

$3x10^6$ HEK293T cells were seeded into 10 cm dishes the day preceding transfection. 2.5 μg of plasmid DNA was transfected into HEK293T cells with Lipofectamine™ 3000 transfection reagent (Invitrogen). After 4 h, 2 μg/ml doxycycline was added to induce gene expression for 24 h prior to co-immunoprecipitation.

Stable cell line production

Lentiviral particles were generated through transfection of HEK293T cells with the lentiviral transfer vector plus four helper plasmids (VSVG, TAT1B, MGPM2, CMV-Rev1B), using TransIT-293 transfection reagent (Mirus) according to the manufacturer's recommendations. Viral supernatant was typically harvested 48 h after transfection, cell debris was removed with a 0.22 μm filter, and target cells were transduced for 48 h then subjected to antibiotic selection for two weeks.

CRISPR/Cas9-mediated gene disruption

A pool of three sgRNAs targeting RNF123 or UBAC1 (Synthego) were delivered to low passage HFFF-TERTs by nucleofection using a 4D-X Core unit (Lonza). Immunoblot was used to confirm that expression of the relevant protein had reduced in polyclonal populations of nucleofected cells, which were used for all experiments in this study.

siRNA knockdown

24 h prior to transfection, HFFF-TERTs were plated in 6- or 12-well plates. Cells were transfected with a pool of DMXL1 siRNAs (L-012091-01-0005, Dharmacon) or control (D-001810-10, Dharmacon) at a final concentration of 50 nM for 24 h, followed by 50 nM DMXL1 or control siRNAs for another 24 h. After 48 h, cells were harvested for immunoblot or lysosomal pH measurement. For viral release assays, where required, HFFF-TERTs were transfected with 100 nM DMXL1 or control siRNA for 24 h, followed by 50 nM siRNAs for another 24 h prior to infection.

Proteomic analyses

Whole cell lysate protein digestion

Cells were washed twice with phosphate buffered saline (PBS), and 250 μl lysis buffer added (6M Guanidine/50 mM HEPES pH 8.5). Cell lifters (Corning) were used to scrape cells in lysis buffer, which was removed to an eppendorf tube, vortexed extensively then sonicated. Cell debris was removed by centrifuging at 21,000 g for 10 min twice. Dithiothreitol (DTT) was added to half of the sample to a final concentration of 5mM and incubated at room temperature for 20 mins. Cysteines were alkylated with 15 mM iodoacetamide and incubated for 20 min at room temperature in the dark. Excess iodoacetamide was quenched with DTT for 15 mins. Samples were diluted with 200 mM HEPES pH 8.5 to 1.5 M Guanidine followed by digestion at room temperature for 3 h with LysC protease at a 1:100 protease-to-protein ratio. Samples were further diluted with 200mM HEPES pH8.5 to 0.5 M Guanidine. Trypsin was then added at a 1:100 protease-to-protein ratio followed by overnight incubation at 37°C. The reaction was quenched with 5% formic acid and centrifuged at 21,000 g for 10 min to remove undigested protein. Peptides were subjected to C18 solid-phase extraction (SPE, Sep-Pak, Waters) and vacuum-centrifuged to near-dryness.

Peptide labelling with tandem mass tags (TMT)

In preparation for TMT labelling, desalted peptides were dissolved in 200mM HEPES pH8.5. Peptide concentration was measured by microBCA (Pierce), and 25 μg of peptide labelled with TMT reagent. TMT reagents (0.8 mg) were dissolved in 43 μl anhydrous acetonitrile and 3 μl added to peptide at a final acetonitrile concentration of 30% (v/v). Sample labelling was as indicated in Table S7E. Following incubation at room temperature for 1 h, the reaction was quenched with hydroxylamine to a final concentration

of 0.3% (v/v). TMT-labelled samples were combined at a 1:1:1:1:1:1:1:1:1:1:1:1:1:1:1:1:1:1 ratio. The sample was vacuum-centrifuged to near dryness and subjected to C18 SPE (Sep-Pak, Waters). An unfractionated single shot was analyzed initially to ensure similar peptide loading across each TMT channel, thus avoiding the need for excessive electronic normalization. As all normalization factors were >0.5 and <2, data for each single-shot experiment was analyzed with data for the corresponding fractions to increase the overall number of peptides quantified. Normalization is discussed in 'data analysis' and high pH reversed-phase (HpRP) fractionation is discussed below.

Offline HpRP fractionation

TMT-labelled tryptic peptides were subjected to HpRP fractionation using an Ultimate 3000 RSLC UHPLC system (Thermo Fisher Scientific) equipped with a 2.1 mm internal diameter (ID) x 25 cm long, 1.7 μm particle Kinetix Evo C18 column (Phenomenex). Mobile phase consisted of A: 3% acetonitrile (MeCN), B: MeCN and C: 200 mM ammonium formate pH 10. Isocratic conditions were 90% A/10% C, and C was maintained at 10% throughout the gradient elution. Separations were conducted at 45°C. Samples were loaded at 200 μl/min for 5 min. The flow rate was then increased to 400 μl/min over 5 min, after which the gradient elution proceed as follows: 0-19% B over 10 min, 19-34% B over 14.25 min, 34-50% B over 8.75 min, followed by a 10 min wash at 90% B. UV absorbance was monitored at 280 nm and 15 s fractions were collected into 96 well microplates using the integrated fraction collector. Fractions were recombined orthogonally in a checkerboard fashion, combining alternate wells from each column of the plate into a single fraction, and commencing combination of adjacent fractions in alternating rows. Wells were excluded prior to the start or after the cessation of elution of peptide-rich fractions, as identified from the UV trace. This yielded two sets of 12 combined fractions, A and B, which were dried in a vacuum centrifuge and resuspended in 10 μl MS solvent (4% MeCN/5% formic acid) prior to LC-MS3. 12 set 'A' fractions were used for MS analysis.

LC-MS3. MS data were generated using an Orbitrap Fusion Lumos (Thermo). An Ultimate 3000 RSLC UHPLC machine equipped with a 300 μm internal diameter × 5 mm Acclaim PepMap μ-Precolumn (Thermo) and a 75 μm internal dimeter × 50 cm 2.1 μm particle Acclaim PepMap RSLC analytical column were used. The loading solvent was 0.1% FA. The analytical solvent consisted of 0.1% FA (A) and 80% AcN + 0.1% FA (B). All separations were carried out at 40°C. Samples were loaded at 5 μl/min for 5 min in loading solvent. The analytical gradient consisted of 3-7% B over 3 min, 7-37% B over 173 min, followed by a 4 min wash at 95% B and equilibration at 3% B for 15 min. Each analysis used a MultiNotch MS3-based TMT method.[100,101] The following settings were used: MS1: 380-1500 Th, 120,000 resolution, 2×10^5 automatic gain control (AGC) target, 50 ms maximum injection time. MS2: Quadrupole isolation at an isolation width of mass-to-charge ratio (m/z) 0.7, collision-induced dissociation fragmentation (normalized collision energy (NCE) 34) with ion trap scanning in turbo mode from m/z 120, 1.5×10^4 AGC target, 120 ms maximum injection time. MS3: In Synchronous Precursor Selection mode, the top 10 MS2 ions were selected for higher energy collision dissociation (HCD) fragmentation (NCE 45) and scanned in the Orbitrap at 60,000 resolution with an AGC target of 1×10^5 and a maximum accumulation time of 150 ms. Ions were not accumulated for all parallelisable time. The entire MS/MS/MS cycle had a target time of 3 s. Dynamic exclusion was set to ± 10 ppm for 70 s. MS2 fragmentation was triggered on precursors 5×10^3 counts and above.

Immunoblotting

HFFF-TERTs were used for all experiments. For most immunoblots, cells were washed with ice-cold PBS and lysed for 30 min on ice with a Nonidet P-40 (NP-40) based lysis buffer (50 mM Tris-HCl pH 8.0, 150 mM NaCl, 1 mM EDTA, 10% (v/v) glycerol, 1% (v/v) Triton X-100 and 0.05% (v/v) NP-40) containing Complete Protease Inhibitor Cocktail (Roche).[102] Lysates were reduced with 6X Protein Loading Dye (Tris 375 mM pH 6.8, 12% SDS, 30% glycerol, 0.6 M DTT, 0.06% bromophenol blue) for 5 min at 100°C or 15 min at 75°C. Protein samples were then separated by polyacrylamide gel electrophoresis (PAGE) using 4-15% TGX Precast Protein Gels (Bio-rad), NuPAGE 4–12% Bis-Tris gels (Invitrogen), NuPAGE 3-8% Tris-Acetate gels (Invitrogen), or 10-20% Tricine gels (Invitrogen), then transferred to 0.2 μm nitrocellulose membranes using Trans-Blot Systems (Bio-rad). The following primary antibodies were used: anti-LC3B (1:2500, #ab48394, Abcam), anti-RNF123 (1:200, #sc-101122, Santa-Cruz), anti-UBAC1 (1:3000,#67385-1-Ig, Proteintech), anti-DMXL1 (1:100, #A304-685A, Bethyl Laboratories), anti-HCMV IE1/2 (1:1000, #MAB810R, Merk), anti-glyceraldehyde 3-phosphate dehydrogenase (GAPDH) (1:10,000, #MAB5718, R&D Systems), anti-Calnexin (1:1000, #LS-B6881, LSBio), anti-V5 (1:1000, #D3H8Q, CST). Secondary antibodies were: IRDye 680RD goat anti-mouse (925-68070, LI-COR), IRDye 800CW goat anti-rabbit (925-32211, LI-COR), HRP-linked goat-anti mouse (1:10,000, #115-035-146, Jackson), HRP-linked goat anti-rabbit (1:1000, #7074, CST). Fluorescent signals were detected using a LI-COR Odyssey and HRP signals were detected using Bio-Rad ChemiDoc Imaging Systems, and images were processed using Image Studio Lite (LI-COR) or ImageLab.

Co-immunoprecipitation

Cells were harvested in lysis buffer (50 mM Tris pH 7.5, 300 mM NaCl, 0.5% (v/v) NP40, 1 mM DTT and Roche protease inhibitor cocktail), tumbled for 30 min at 4C and then centrifuged at 15,000 g for 14 min at 4C. The supernatants were incubated for 3 h with immobilized mouse monoclonal anti-V5 agarose resin. Samples were washed multiple times with lysis buffer, followed by incubation in Protein Loading Dye (components see immunoblotting section) for 10 min at 100C, centrifugation at 1000 g for 1 min, then analysis by immunoblotting.

Flow cytometry

Cells were washed in PBS before fixation with 4% PFA fixation buffer (420801 Biolegend) for 15 min at room temperature. 10,000 or 20,000 events were acquired with a Fortessa flow cytometer (Becton Dickinson) and analyzed using FlowJo V9 software (Tree Star Inc).

Immunofluorescence microscopy

For LAMP1-LC3B co-localization analysis, HFFF-TERTs stably expressing US33A or control were seeded onto coverslips and incubated overnight. For LAMP1-LC3B co-localization analysis in the context of HCMV infection, HFFF-TERTs were infected on coverslips with WT or ΔUS33A HCMV at MOI 0.1 for 24 h. For the HCMV vAC formation analysis, HFFF-TERTs were infected on coverslips with WT or ΔUS33A at MOI 1 for 24, 36, 48, 72, or 96 h. Cells were then cross-linked with 4% fixation buffer (Biolegend), permeabilized with ice-cold methanol or 0.5% Triton-X100 (Sigma), and blocked with Human TruStain FcX (Biolegend) or HCMV-serotype negative human serum. Primary antibodies were used as indicated and included: rabbit anti-LC3B (1:1000, #ab43894, Abcam), mouse anti-LAMP1 (1:100, #328602, Biolegend), rabbit anti-Giantin (1:1000, #Ab80864, Abcam) and mouse anti-glycoprotein B (1:1000, #Ab6499, Abcam). Secondary antibodies were anti-mouse Alexa Fluor 647 (1:1000, #A31573, Thermo) and anti-rabbit Alexa Fluor 568 (1:1000, #A-11011, Thermo). Cell nuclei were stained with DAPI (Cell Signaling). Fluorescence was observed using a confocal microscope (Zeiss LSM 880).

Super-resolution live-cell imaging

HFFF-TERTs expressing US33A or control were transfected with mCherry-LC3[92] and CD63-GFP plasmids (kind gift of Prof Paul Luzio, Cambridge Institute for Medical Research) by nucleotransfection using a 4D-X core unit (Lonza). After 72 h, cells were starved with serum-free DMEM for 30 min and imaged every 2 s for 3 min using the AiryScan function of a Zeiss LSM880 confocal microscope, with a 63x objective.

RT-qPCR

Total RNA from mock-, HCMV- or Adenovirus-infected HFFF-TERTs was extracted using RNeasy Mini Kit (Qiagen). cDNA was synthesized using GoScript Reverse Transcriptase (Promega). To detect US33A or truncated versions of US33A-V5, qPCR was performed using Fast SYBR Green Master Mix (Applied Biosystems). Primers targeting HCMV US33A, US33A-V5 or GAPDH and 18S (as an internal control) are shown in the Table S7F. The PCR program started with activation at 95C for 2 min, followed by 40 cycles of denaturation at 95C for 5 s and annealing/extension at 60C for 30 s. To detect DMXL1, qPCR was performed using TaqMan primers (Invitrogen, Assay ID: Hs00194128_m1 for DMXL1, Assay ID: Hs02786624_g1 for GAPDH) and TaqMan Universal PCR Master Mix (Invitrogen). The PCR program started with activation at 50C for 2 min and 95C for 10 min, followed by 40 cycles of denaturation at 95C for 15 s and annealing/extension at 60C for 1 min. Melting curve analyses were performed to verify the amplification specificity. All mock-infected samples exhibited non-singular melting curves, indicating non-specific amplification; values for these samples were set to zero.

Lysosomal pH measurements

For LysoTracker analysis, cells were stained with 100 nM LysoTracker Red DND-99 (L7528 Invitrogen) at 37C for 30 min, washed with PBS, fixed with 4% PFA fixation buffer (420801 Biolegend) and imaged using flow cytometry or microscopy.

For LysoSensor analysis, cells were stained with 5 μM LysoSensor Yellow/Blue DND-160 (L7545 Invitrogen) at room temperature for 10 min. LysoSensor was removed, cells were washed three times with PBS then recovered in phenol-red free DMEM (Gibco 31053028) for 15 min. Fluorescence intensity was quantified using a plate reader (CLARIOSTAR) at two excitation wavelengths, 340 nm ($F_{340\ nm}$) and 380 nm ($F_{380\ nm}$), with the emission wavelength set at 527 nm.[31] Five independent wells were analyzed for each condition to calculate an average $F_{340\ nm}/F_{380\ nm}$ for each independent experiment. Images of LysoSensor staining were captured at two emission wavelengths, 430 ± 25 nm and 465 ± 30 nm.

Plaque assay

1.3×10^5 HFFF-TERTs stably expressing shRNA constructs targeted against DMXL1 or control were seeded in 12-well plates in triplicate 24 h prior to infection with AD169-GFP at MOI 0.005. After 2 h, media was replaced with a 1:1 (v/v) mixture of 2 x DMEM and Avicel (2% w/v in water, FMC BioPolymer). After two weeks, the DMEM/Avicel mixture was removed, and cells were washed three times with PBS before fixation in 4% (w/v) paraformaldehyde. The number of GFP-fluorescent plaques per well was counted and an average calculated across three independent wells for each condition.

Plaque size analysis

Images of 12 plaques per well were taken using a Zeiss AxioObserver inverted fluorescence microscope at 5 x magnification. The first 12 plaques encountered that were suitable for imaging were used. Suitable plaques were those that fitted entirely in the field of view, were not located against the edge of the well, and were the only plaque within the field of view. Images were converted into greyscale and plaque area was calculated using Image J Fiji.

Viral release assay

HFFF-TERTs were infected with WT or ΔUS33A HCMV, or HSV-1 at MOI 0.1. After 6 days (for HCMV infection) or 24 h (for HSV-1 infection), cell culture medium was harvested, containing released virus. Infected cells were detached using trypsin, followed by sonication to release cell-associated virus, using a UP2000St Ultrasonic lab homogenizer (Hielscher). The program was: 210 W (100% power), 100% pulse, 100% amplitude, 30 sec, 3 cycles. Cell debris were removed by centrifugation at 500 g for 10 min. Released or cell-associated virus was titered on a fresh batch of HFFF-TERTs using the method described in the 'Viruses' section. 10,000 events were acquired with a Fortessa flow cytometer (Becton Dickinson) flow cytometer and analyzed with FlowJo V9 software, to assess %GFP positive cells. In order to combine data from three independent replicate experiments, and to account for variation in absolute titer, relative titers were calculated for each experiment and then averaged. Four conditions were examined: (a) WT, released virus; (b) ΔUS33A, released virus; (c) WT, cell associated virus; (d) ΔUS33A, cell associated virus. For (a), the relative titer was calculated as: (a) / $\sum$((a) + (b) + (c) + (d)). Similar calculations were performed for (b), (c) and (d). Mean relative titres for (a), (b), (c) and (d) were then calculated.

QUANTIFICATION AND STATISTICAL ANALYSIS

Data analysis

Mass spectra were processed using a Sequest-based software pipeline for quantitative proteomics, ''MassPike'', through a collaborative arrangement with Professor Steven Gygi's laboratory at Harvard Medical School. MS spectra were converted to mzXML using an extractor built upon Thermo Fisher's RAW File Reader library (version 4.0.26). In this extractor, the standard mzxml format has been augmented with additional custom fields that are specific to ion trap and Orbitrap mass spectrometry and essential for TMT quantitation. These additional fields include ion injection times for each scan, Fourier Transform-derived baseline and noise values calculated for every Orbitrap scan, isolation widths for each scan type, scan event numbers, and elapsed scan times. This software is a component of the MassPike software platform and is licensed by Harvard Medical School.

A combined database was constructed from (a) the human Uniprot database (26th January, 2017), (b) the HCMV strain Merlin Uniprot database, (c) all additional non-canonical human cytomegalovirus ORFs described by Stern-Ginossar et al.,[103] (d) a six-frame translation of HCMV strain Merlin filtered to include all potential ORFs of $\geq$8 amino acids (delimited by stop-stop rather than requiring ATG-stop) and (e) common contaminants such as porcine trypsin and endoproteinase LysC. ORFs from the six-frame translation (6FT-ORFs) were named as follows: 6FT_Frame_ORFnumber_length, where Frame is numbered 1-6, and length is the length in amino acids. The combined database was concatenated with a reverse database composed of all protein sequences in reversed order. Searches were performed using a 20-ppm precursor ion tolerance. Fragment ion tolerance was set to 1.0 Th. TMT tags on lysine residues and peptide N termini (Experiment 1: 229.162932 Da; Experiments 2-3: 304.2071 Da) and carbamidomethylation of cysteine residues (57.02146 Da) were set as static modifications, while oxidation of methionine residues (15.99492 Da) was set as a variable modification.

To control the fraction of erroneous protein identifications, a target-decoy strategy was employed.[104] Peptide spectral matches (PSMs) were filtered to an initial peptide-level false discovery rate (FDR) of 1% with subsequent filtering to attain a final protein-level FDR of 1%. PSM filtering was performed using a linear discriminant analysis, as described previously.[104] This distinguishes correct from incorrect peptide IDs in a manner analogous to the widely used Percolator algorithm (https://noble.gs.washington.edu/proj/percolator/), though employing a distinct machine-learning algorithm. The following parameters were considered: XCorr, ΔCn, missed cleavages, peptide length, charge state, and precursor mass accuracy.

Protein assembly was guided by principles of parsimony to produce the smallest set of proteins necessary to account for all observed peptides (algorithm described in Huttlin et al.[104]). Where all PSMs from a given HCMV protein could be explained either by a canonical gene or non-canonical ORF, the canonical gene was picked in preference. In a small number of cases, PSMs assigned to a non-canonical or 6FT-ORF were a mixture of peptides from the canonical protein and the ORF. This most commonly occurred where the ORF was a 5′-terminal extension of the canonical protein (thus meaning that the smallest set of proteins necessary to account for all observed peptides included the ORFs alone). In these cases, the peptides corresponding to the canonical protein were separated from those unique to the ORF, generating two separate entries. In a single case, PSM were assigned to the 6FT-ORF 6FT_6_ORF1202_676aa, which is a 5'-terminal extension of the non-canonical ORF ORFL147C. The principles described above were used to separate these two ORFs.

Proteins were quantified by summing TMT reporter ion counts across all matching peptide-spectral matches using ''MassPike'', as described previously.[100] Briefly, a 0.003 Th window around the theoretical m/z of each reporter ion (127n, 128n, 130c) was scanned for ions and the maximum intensity nearest to the theoretical m/z was used. The primary determinant of quantitation quality is the number of TMT reporter ions detected in each MS3 spectrum, which is directly proportional to the signal-to-noise (S:N) ratio observed for each ion. An isolation specificity filter with a cut-off of 50% was additionally employed to minimize peptide co-isolation.[100] Peptide-spectral matches with poor quality MS3 spectra (a combined S:N ratio of less than 250 across all TMT reporter ions) or no MS3 spectra at all were excluded from quantitation. Peptides meeting the stated criteria for reliable quantitation were then summed by parent protein, in effect weighting the contributions of individual peptides to the total protein signal based on their individual TMT reporter ion yields. Protein quantitation values were exported for further analysis in Excel.

For protein quantitation, reverse and contaminant proteins were removed, then each reporter ion channel was summed across all quantified proteins and normalized assuming equal protein loading across all channels. For further analysis and display in Figures, fractional TMT signals were used (i.e. reporting the fraction of maximal signal observed for each protein in each TMT channel, rather than the absolute normalized signal intensity). This effectively corrected for differences in the numbers of peptides observed per protein. For the TMT-based experiments, normalized S:N values are presented in Table S1. As it was not possible confidently to assign peptides to only two HLA-A, -B or -C alleles, signal:noise values were further summed for each of these alleles to give a single combined result for each of HLA-A, -B or -C.

For each protein in the single viral gene-deletion and overexpression screen, a mean (μ) and standard deviation (σ) for all paired, summed S:N values was calculated (i.e. sum of both ΔUS29 replicates, sum of both ΔUS30 replicates, sum of both ΔUS31 replicates…). In each case, the maximum (x) value was omitted. For example, for DMXL1 in Figure 1E, μ and σ were calculated for WT, ΔUS29, ΔUS30, ΔUS31, ΔUS32, ΔUS34, ΔUS34A but not the maximum ΔUS33A. The formula $Z = (x-\mu) / \sigma$ was then applied to calculate the z-score. Fold change compared to WT infection or control vector expression was calculated from normalized S:N values using FC = Δx / WT or x / control. For Figure S3A, p-values were estimated using the method of Significance A.[105]

Pathway analysis

The Database for Annotation, Visualization and Integrated Discovery (DAVID) was used to determine functional enrichment of Gene Ontology biological process terms and UniProt Keywords.[93] A given cluster was always searched against a background of all proteins quantified within the relevant experiment. For Table S2, DAVID analysis examined proteins rescued by each gene deletion compared to control by >1.5-fold with a z-score >3. The AimGO vacuolar acidification database (accession: GO:0007035) was used to overlap with our prior databases of protein degraded early and late during HCMV infection.[7,8] For the former, 133 proteins degraded with medium confidence were considered, and for the latter, 30 additional proteins degraded as defined in Fletcher-Etherington et al. were considered.[8]

Immunofluorescence microscopy analysis

To quantify the LAMP1-LC3B co-localization, at least 10 images with over five cells were analyzed for each sample of each experiment (details see RESULT). Pearson's coefficients of defined region of interest (ROI) were examined with Volocity software as quantification of co-localization, with a threshold automatically assigned based on a study by Costes et al.[106] (Table S5). ROI of HFFF-TERTs expressing US33A or control was defined as an entried image, and that of HCMV infected cells was defined by drawing outline of regions with GFP signals.

Abundance of LAMP1 and LC3B in HFFF-TERTs expressing US33A or control, or infected cells was quantified by measurement of mean intensity of ROI using ImageJ. ROI was defined by HCS CellMask™ Blue Stain (Invitrogen) for HFFF-TERTs expressing US33A or control, and GFP signal for HCMV infection using auto-threshold with Huang method.

AlphaFold2 prediction

Potential structures and per-residue local distance difference test (pLDDT) confidence scores for the US33A protein (Uniprot accession: F7V999) were predicted using AlphaFold2 (AF2).[107] Structures were visualized and generated using PyMol Molecular Graphics System (http://www.pymol.org).